JACC: BASIC TO TRANSLATIONAL SCIENCE VOL. 8, NO. 8, 2023

ORIGINAL RESEARCH - PRECLINICAL

Glucagon-Like Peptide-1 Protects Against Atrial Fibrillation and Atrial Remodeling in Type 2 Diabetic Mice

Loryn J. Bohne, PhD, Hailey J. Jansen, PhD, Tristan W. Dorey, PhD, Irene M. Daniel, BHSc, K. Lockhart Jamieson, PhD, Darrell D. Belke, PhD, Megan D. McRae, BHSc, Robert A. Rose, PhD

VISUAL ABSTRACT

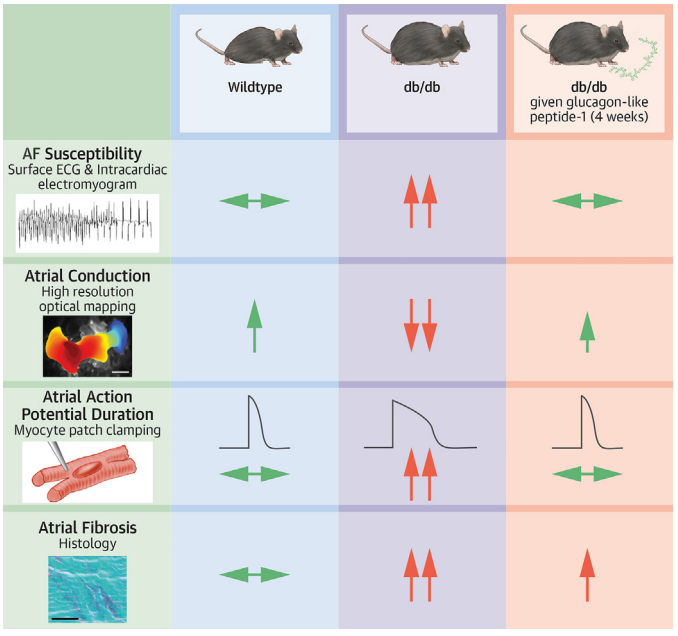

Bohne LJ, et al. J Am Coll Cardiol Basic Trans Science. 2023;8(8):922-936.

HIGHLIGHTS

- **AF is highly prevalent in type 2 diabetes mellitus where it increases morbidity and mortality.**
- **GLP-1R agonists are used to treat T2DM, but their effects on AF are unclear.**
- **T2DM db/db mice are highly susceptible to AF in association with atrial electrical and structural remodeling.**
- **GLP-1 and liraglutide (GLP-1R agonist) prevented AF as well as atrial remodeling in db/db mice.**
- **GLP-1R agonists may represent a therapeutic option to prevent AF in patients with T2DM.**

From the Libin Cardiovascular Institute, Cumming School of Medicine, University of Calgary, Calgary, Alberta, Canada; Department of Cardiac Sciences, Cumming School of Medicine, University of Calgary, Calgary, Alberta, Canada; and the Department of Physiology and Pharmacology, Cumming School of Medicine, University of Calgary, Calgary, Alberta, Canada.
The authors attest they are in compliance with human studies committees and animal welfare regulations of the authors' institutions and Food and Drug Administration guidelines, including patient consent where appropriate. For more information, visit the Author Center.

Manuscript received October 17, 2022; revised manuscript received January 4, 2023, accepted January 4, 2023.

ISSN 2452-302X https://doi.org/10.1016/j.jacbts.2023.01.005

SUMMARY

Atrial fibrillation (AF) is highly prevalent in type 2 diabetes where it increases morbidity and mortality. Glucagon-like peptide (GLP)-1 receptor agonists are used in the treatment of type 2 diabetes (T2DM), but their effects on AF in T2DM are poorly understood. The present study demonstrates type 2 diabetic db/db mice are highly susceptible to AF in association with atrial electrical and structural remodeling. GLP-1, as well as the long-acting GLP-1 analogue liraglutide, reduced AF and prevented atrial remodeling in db/db mice. These data suggest that GLP-1 and related analogues could protect against AF in patients with T2DM.

ABBREVIATIONS AND ACRONYMS

4-AP = 4-aminopyridine

AERP = atrial effective refractory period

AF = atrial fibrillation

AP = action potential

APD = action potential duration

AVERP = atrioventricular node effective refractory period

cSNRT = corrected sinoatrial node recovery time

ECG = electrocardiogram

GLP = glucagon-like peptide

GLP-1R = glucagon-like peptide 1 receptor

I_K = K^+ current

I_{Kur} = ultra-rapid delayed rectifier K^+ current

I_{Na} = Na^+ current

I_{to} = transient outward K^+ current

SAN = sinoatrial node

T2DM = type 2 diabetes mellitus

Atrial fibrillation (AF) is highly prevalent in patients with type 2 diabetes mellitus (T2DM), which accounts for ~90% of the diabetic population.[1-4] With obesity occurring at epidemic proportions, T2DM and AF occurrence are expected to continue to rise. AF is associated with increased risk of stroke and death, as well as severe impairments in quality of life.[5] In addition, patients with T2DM that develop AF experience substantial increases in total mortality, cardiovascular death, and stroke compared to patients who are diabetic without AF.[4,6] Current therapeutic approaches for AF, including in T2DM, are limited.

AF can develop in association with electrical and structural remodeling of the atria.[7-9] Atrial action potential (AP) morphology is a critical determinant of susceptibility to AF and can be affected by electrical remodeling. Specifically, the AP upstroke is determined by the Na^+ current (I_{Na}) (carried by $Na_V1.5$ channels), which importantly affects atrial conduction velocity.[7,10] Changes in conduction velocity can affect susceptibility to re-entry and AF occurrence. Action potential duration (APD) is determined in part by several repolarizing K^+ currents including the transient outward K^+ current (I_{to}) (carried by $K_V4.2$ and $K_V4.3$), the ultrarapid delayed rectifier K^+ current (IK_{ur}) (carried by $K_V1.5$ channels), and the inward rectifier K^+ current (I_{K1}) (carried by $K_{ir}2$ channels).[10] Alterations in these currents can lead to changes in APD that can also favor re-entry or triggered activity in AF.[7,9]

Changes in atrial electrical conduction can also result from structural remodeling caused by fibrosis following enhanced collagen production and deposition.[7,8] This inappropriate collagen deposition can disrupt connectivity between myocytes leading to slow or irregular conduction, which can further promote re-entry and favor AF development. Recent studies have demonstrated that the db/db mouse model of T2DM is characterized by increased susceptibility to AF caused by impaired atrial conduction in association with electrical and structural remodeling in the atria.[11]

Glucagon-like peptide (GLP)-1 is an incretin hormone produced in endocrine cells in the gut that mediates effects via the glucagon-like peptide 1 receptor (GLP-1R).[12,13] GLP-1 can contribute to blood glucose regulation via insulinotropic effects; however, GLP-1R agonists also have a number of additional beneficial actions including in the cardiovascular system.[14-16] GLP-1R is highly expressed in the atria of the heart,[13,17] suggesting that GLP-1 may be important in regulating atrial function. A number of GLP-1R agonists have been developed for therapeutic use in patients with T2DM, including liraglutide, which is a long-acting form of GLP-1 with a half-life of 13 hours compared to ~2 minutes for native GLP-1.[13,18]

Clinical studies have shown that GLP-1R agonists such as liraglutide do not increase the incidence of AF in T2DM,[4] and some studies have suggested that GLP-1R agonists could reduce the risk of AF in diabetes.[16,19] Liraglutide has also been shown to protect against AF in a nondiabetic canine model of AF.[20] Overall, however, whether GLP-1 or GLP-1R agonists are protective against AF in T2DM, and the mechanisms involved, are poorly understood. Accordingly, the purpose of this study was to investigate the effects of chronic GLP-1 treatment on AF susceptibility, as well as atrial remodeling, in type 2 diabetic db/db mice.

METHODS

An expanded Methods section can be found in the Supplemental Appendix.

MICE. This study used male and female littermate wild-type and db/db mice[21] aged 16-20 weeks. All experimental procedures were approved by the

University of Calgary Animal Care and Use Committee and conformed to the guidelines of the Canadian Council on Animal Care as described in the Supplemental Appendix.

For chronic GLP-1 studies, db/db mice were treated with GLP-1 (7-36 amide; 15 μg/kg/d), or saline as a control, via osmotic minipumps, for 4 weeks beginning at 12-16 weeks of age. This dose of GLP-1 was chosen based on studies showing that similar GLP-1 doses and treatment durations have protective effects in mouse models of diabetes.[22] For chronic liraglutide studies, db/db mice were given subcutaneous injections of liraglutide (0.25 mg/kg/d), or vehicle control, once per day for 28 to 30 days beginning at 12 to 16 weeks of age. This dose of liraglutide was calculated to be equivalent to the dose used in obese humans.[16,23] Additional details are available in the Supplemental Appendix.

Blood glucose levels were assessed by oral glucose tolerance tests. Plasma insulin levels were measured using commercially available assays. Blood pressure was monitored by tail-cuff plethysmography. Cardiac structure and function were assessed by echocardiography. Additional details are available in the Supplemental Appendix.

IN VIVO ELECTROPHYSIOLOGY. Surface electrocardiograms (ECGs) were measured in anesthetized mice using subdermal needle electrodes. In conjunction, a 1.2-F octapolar electrophysiology catheter was inserted into the right heart via an incision in the jugular vein and used to measure AF susceptibility, atrial effective refractory period (AERP), atrioventricular node effective refractory period (AVERP), and corrected sinoatrial node (SAN) recovery time (cSNRT) as described previously.[24-26] AF was defined as a rapid and irregular atrial rhythm (fibrillatory baseline in the ECG) with irregular RR intervals lasting at least 1 second. Additional details are provided in the Supplemental Appendix.

HIGH-RESOLUTION OPTICAL MAPPING. Activation patterns, atrial conduction velocities, and atrial optical APD were measured in isolated atrial preparations using high-resolution optical mapping as described previously[24,27] and in the Supplemental Appendix.

PATCH-CLAMPING OF ISOLATED ATRIAL MYOCYTES. Isolated left and right atrial myocytes were used to record stimulated APs and ionic currents including I_{Na}, total I_K, I_{to}, and I_{Kur} using the whole-cell patch-clamp technique as described previously[24,25] and in the Supplemental Appendix.

QUANTITATIVE POLYMERASE CHAIN REACTION. Expression of messenger RNA for *Kcnd2*, *Kcnd3*, *Kcnip2*, *Kcna5*, *Col1a*, *Col3a*, and *Hprt1* (reference gene) was measured in left atrial tissue samples using approaches previously described.[24,25] Primer sequences and experimental protocols are described in the Supplemental Appendix.

WESTERN BLOTTING. Western blotting for $K_v4.2$, $K_v4.3$, KChIP2, and $K_v1.5$ was performed in left atrial tissue samples as described previously.[11] Additional details are provided in the Supplemental Appendix.

HISTOLOGY. Interstitial collagen levels were measured using picrosirius red (collagen) and fast green (myocardium) staining of paraffin embedded sections (5 μm) through the left and right atria. Fibrosis was quantified using ImageJ software (National Institutes of Health).

STATISTICAL ANALYSIS. Data are presented as mean ± SEM. Categorical data were compared using Fisher exact test and continuous data were compared using one-way or two-way analysis of variance with Holm-Sidak post hoc test for multiple pairwise comparisons as indicated in each figure legend. Data were assessed for normality using Shapiro-Wilks test. Statistical differences are reported as $P < 0.05$, $P < 0.01$, or $P < 0.001$.

RESULTS

EFFECTS OF CHRONIC GLP-1 TREATMENT ON AF SUSCEPTIBILITY AND ATRIAL ELECTROPHYSIOLOGY IN DB/DB MICE. Compared to wild-type mice, db/db mice infused with saline for 4 weeks (db/db_{saline}) exhibited increased blood glucose levels (Supplemental Figures 1A to 1C). Four weeks of GLP-1 (15 μg/kg/d) treatment in db/db mice ($db/db_{GLP\text{-}1}$) resulted in intermediate blood glucose levels that were between those of wild-type and db/db_{saline} mice (Supplemental Figures 1A to 1C). Body mass and plasma insulin concentrations were similarly increased in db/db_{saline} and $db/db_{GLP\text{-}1}$ mice compared with in wild-type mice (Supplemental Figures 1D and 1E). There were no differences in blood pressure between treatment groups at baseline or after 4 weeks of GLP-1 treatment (Supplemental Figure 2). Echocardiography demonstrated an increase in maximum left atrial area in db/db_{saline} mice; however, there were no other differences in atrial area in db/db_{saline} mice compared with in wild-type mice. There were also no effects of GLP-1 on atrial area compared with that of db/db_{saline} mice (Supplemental Table 1).

FIGURE 1 Effects of chronic GLP-1 Treatment on AF and AERP in db/db Mice

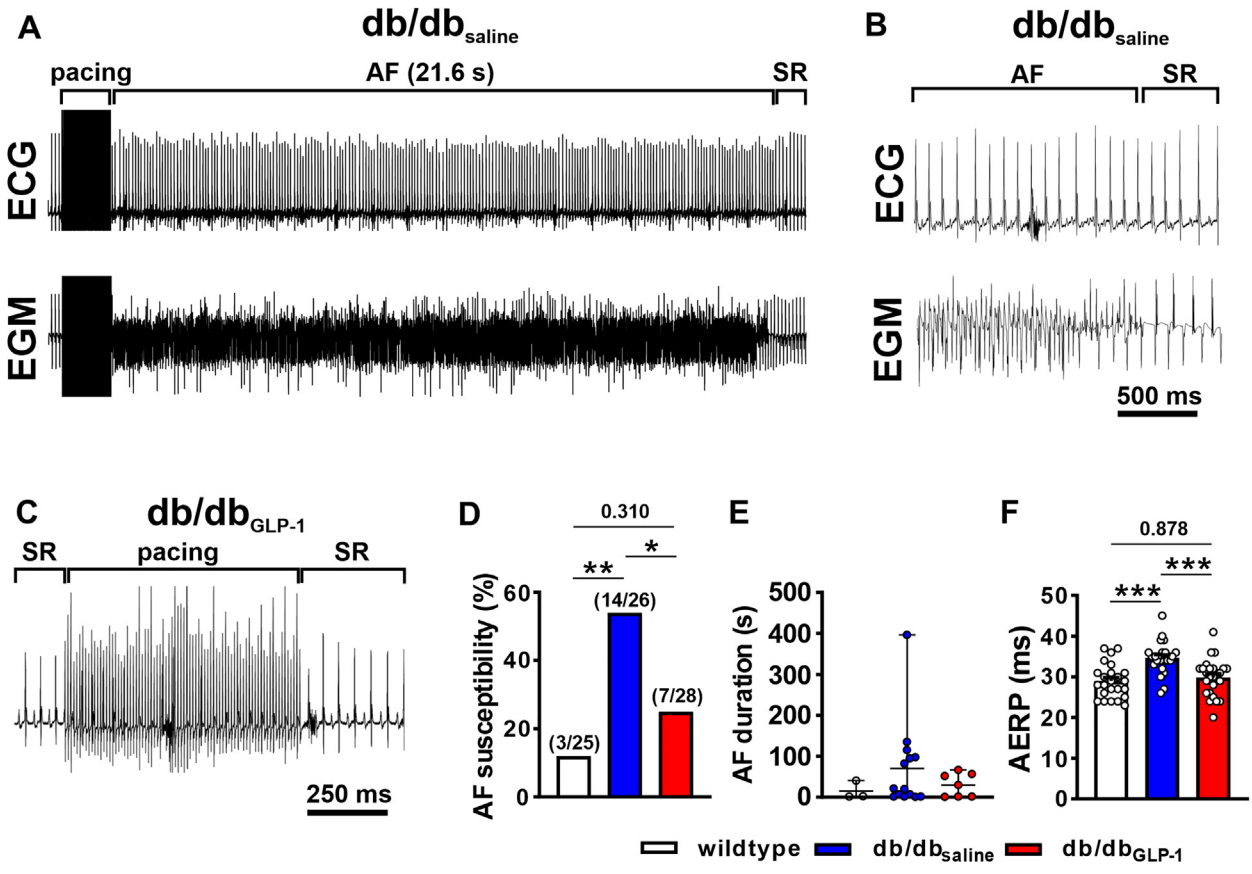

(A) Representative surface electrocardiogram (ECG) **(top)** and atrial intracardiac electrogram (EGM) **(lower)** showing the induction of atrial fibrillation (AF) following burst pacing in an anesthetized db/db mouse after 4 weeks of saline infusion. AF lasted for 21.6 seconds and then reverted to sinus rhythm (SR). **(B)** Magnified view of the recording shown in **A** illustrating AF converting to SR. **(C)** Representative surface ECG showing the absence of AF induction after burst pacing in a db/db mouse infused with glucagon-like peptide-1 (GLP-1) for 4 weeks. **(D)** Inducibility of AF in wild-type mice, db/db mice infused with saline (db/db_{saline}), and db/db mice infused with GLP-1 (db/db_{GLP-1}) for 4 weeks. Numbers in parentheses indicate the number of mice induced into AF. Data analyzed by Fisher exact test. **(E)** Duration of AF in the wild-type, db/db_{saline}, and db/db_{GLP-1} mice that were induced into AF. **(F)** Atrial effective refractory period (AERP) in wild-type (n = 25), db/db_{saline} (n = 26), and db/db_{GLP-1} (n = 28) mice. Data analyzed by one-way analysis of variance with Holm-Sidak post hoc test. *$P < 0.05$, **$P < 0.01$, ***$P < 0.001$.

Furthermore, there were no differences between groups in measures of ventricular structure or function (Supplemental Table 1).

Atrial burst pacing in anesthetized mice (**Figures 1A to 1C**) demonstrates that AF susceptibility was increased in db/db_{saline} mice compared with wild-type mice and that this elevated susceptibility to AF was prevented in db/db_{GLP-1} mice (**Figure 1D**). When AF was induced, it was longer on average in db/db_{saline} mice, whereas wild-type and db/db_{GLP-1} mice exhibited shorter AF durations on average (**Figure 1E**). Programmed electrical stimulation studies demonstrate that AERP was increased in db/db_{saline} mice compared with wild-type mice and GLP-1 treatment prevented this increase in AERP in db/db mice (**Figure 1F**). cSNRT was also prolonged in db/db_{saline} mice and not significantly affected by GLP-1 treatment (Supplemental Table 2).

Surface ECG analysis (**Figures 2A and 2B**, Supplemental Table 2) demonstrates that P-wave duration as well as PR interval were increased in male and female db/db_{saline} mice (**Figure 2C**). These increases were largely prevented in db/db_{GLP-1} although P-wave duration was still longer in db/db_{GLP-1} mice compared with in wild-type mice (**Figure 2C**). In contrast, there were no effects of GLP-1 treatment on QRS duration, QT interval, or AVERP in db/db mice (Supplemental Table 1). These effects of GLP-1 on ECG

FIGURE 2 Effects of Chronic GLP-1 Treatment on P-Wave Duration in db/db Mice

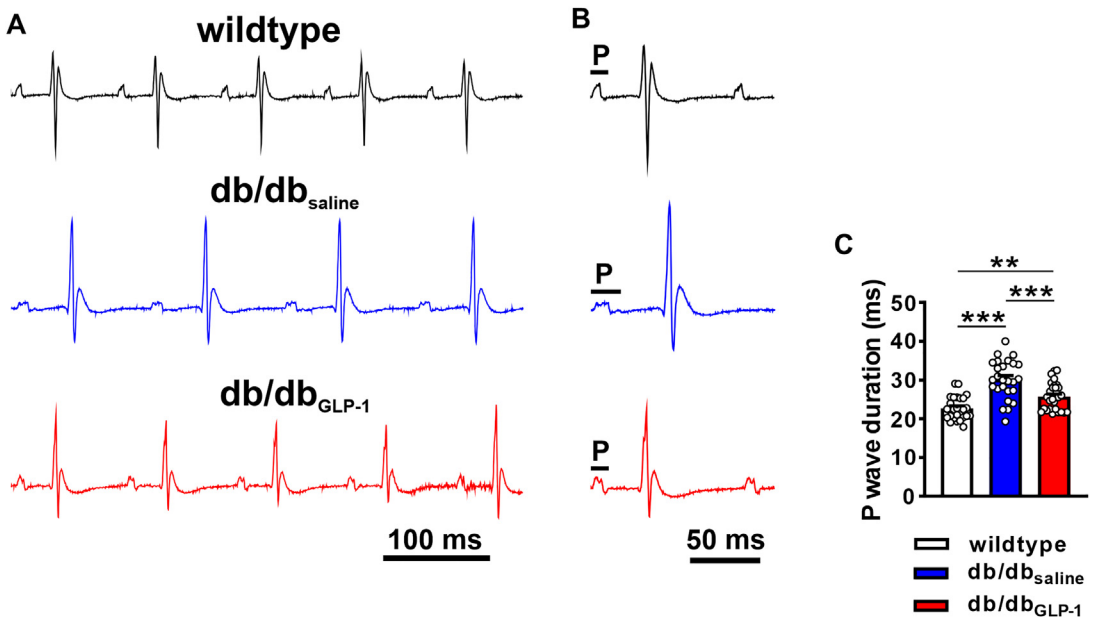

(A) Representative surface ECGs in anesthetized wild-type, db/db$_{saline}$, and db/db$_{GLP-1}$ mice. **(B)** Magnified ECGs in wild-type, db/db$_{saline}$, and db/db$_{GLP-1}$ mice illustrating differences in P-wave duration. **(C)** Summary of P-wave duration in wild-type (n = 25), db/db$_{saline}$ (n = 26), and db/db$_{GLP-1}$ (n = 28) mice. Data analyzed by one-way analysis of variance with Holm-Sidak post hoc test. Refer to Supplemental Tables 2 to 4 for additional ECG analyses. $^{**}P < 0.01$, $^{***}P < 0.001$. Abbreviations as in Figure 1.

parameters were comparable between male and female mice (Supplemental Tables 3 and 4); therefore, male and female data were combined in all studies.

EFFECTS OF CHRONIC LIRAGLUTIDE TREATMENT ON AF SUSCEPTIBILITY AND ATRIAL ELECTROPHYSIOLOGY IN DB/DB MICE. To test the impact of targeting the GLP-1 pathway in a more clinically relevant fashion, db/db mice were treated with the long-acting GLP-1 analogue liraglutide by once daily subcutaneous injection (0.25 mg/kg/d). Vehicle-injected db/db mice (db/db$_{veh}$) were hyperglycemic compared to wild-type mice, whereas db/db mice treated with liraglutide (db/db$_{lira}$) showed reduced blood glucose levels, although not fully to wild-type levels (Supplemental Figure 3A to 3C). Body mass was similarly elevated in db/db mice injected with vehicle or liraglutide at baseline; however, after 4 weeks of treatment, body mass was lower in db/db$_{lira}$ mice compared with in db/db$_{veh}$ mice, although still increased compared to wild-type mice (Supplemental Figure 3D). Plasma insulin levels were similarly elevated in db/db$_{veh}$ and db/db$_{lira}$ mice (Supplemental Figure 3E).

Vehicle-injected db/db mice exhibited an increased susceptibility to burst pacing induced AF that was longer lasting than for wild-type mice (**Figures 3A to 3C**). In contrast, db/db$_{lira}$ mice had an intermediate susceptibility to AF between wild-type and db/db$_{veh}$ mice that on average was shorter in duration than for db/db$_{veh}$ mice (**Figures 3B and 3C**). AERP was increased in db/db$_{veh}$ mice compared with wild-type mice, and this was prevented in db/db$_{lira}$ mice (**Figure 3D**). P-wave duration was also increased in db/db$_{veh}$ mice compared with in wild-type and normalized in db/db$_{lira}$ mice (**Figures 4A to 4C**). Similar to GLP-1, liraglutide had no effects on ventricular ECG intervals, cSNRT, or AVERP in db/db mice (Supplemental Table 5).

EFFECTS OF CHRONIC GLP-1 ON ATRIAL CONDUCTION AND ATRIAL OPTICAL AP MORPHOLOGY. Changes in P-wave duration are indicative of altered atrial conduction; therefore, this was directly assessed in isolated atrial preparations paced at 8 Hz using optical mapping. Activation maps show that atrial conduction time was longer in db/db$_{saline}$ mice than in wild-type mice and that this was shortened in db/db$_{GLP-1}$ mice (**Figure 5A**). Right and left atrial conduction velocities were reduced in db/db$_{saline}$ mice compared with wild-type mice, but conduction

FIGURE 3 Effects of Chronic Liraglutide Treatment on AF and AERP in db/db Mice

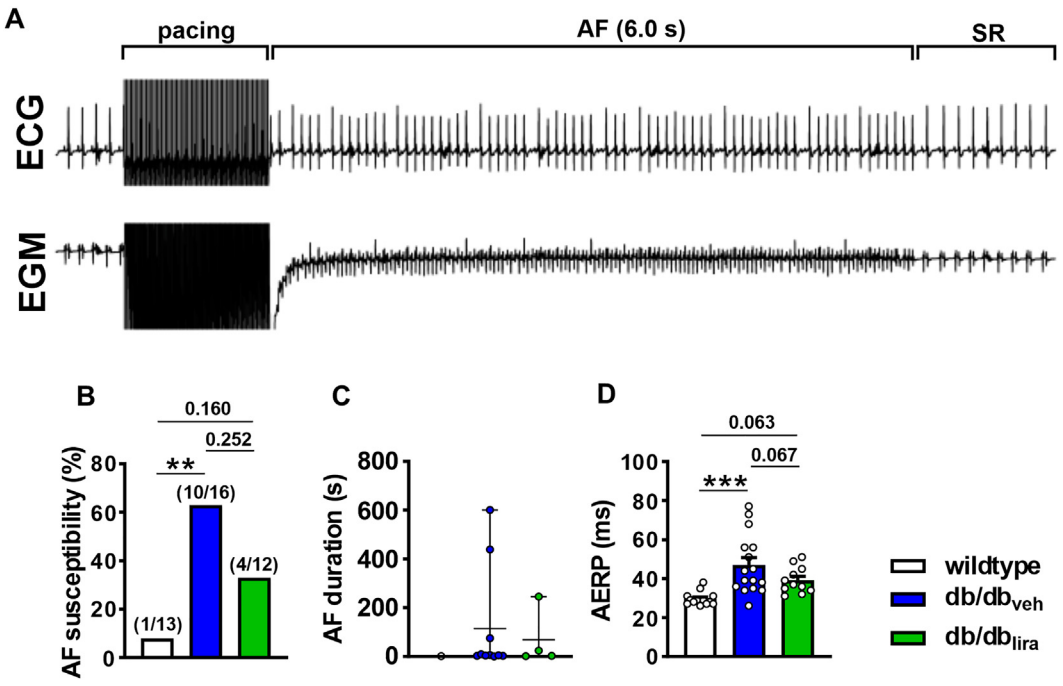

(A) Representative surface ECG **(top)** and atrial intracardiac EGM **(bottom)** showing induction of AF and conversion to SR in a vehicle-injected db/db mouse. **(B)** Inducibility of AF in wild-type mice, db/db mice given daily vehicle injections (db/db$_{veh}$), and db/db mice given daily injections of liraglutide for 4 weeks (db/db$_{lira}$). Numbers in parentheses indicate the number of mice induced into AF. Data analyzed by Fisher exact test. **(C)** Duration of AF in wild-type, db/db$_{veh}$, and db/db$_{lira}$ mice that were induced into AF. **(D)** AERP in wild-type (n = 13), db/db$_{veh}$ (n = 16), and db/db$_{lira}$ (n = 11) mice. Data analyzed by one-way analysis of variance with Holm-Sidak post hoc test. $^{**}P < 0.01$, $^{***}P < 0.001$. Abbreviations as in Figure 1.

velocities were substantially improved in db/db$_{GLP\text{-}1}$ mice (Figures 5B and 5C). Representative optical APs (Figure 5D) and APD maps (Figure 5E) demonstrate changes in APD in db/db mice treated with GLP-1. Specifically, right and left atrial APD_{50} (Figures 5F and 5G) and APD_{70} (Figures 5H and 5I) were increased in db/db$_{saline}$ mice compared with wild-type mice and normalized in db/db$_{GLP\text{-}1}$ mice. Similar changes in atrial conduction and APD were observed in optical mapping experiments in atrial preparations in sinus rhythm (ie, no pacing) (Supplemental Figure 4).

EFFECTS OF CHRONIC GLP-1 ON ATRIAL MYOCYTE ELECTROPHYSIOLOGY IN DB/DB MICE. AP recordings in isolated left atrial myocytes (Figure 6A) revealed increases in cell capacitance in db/db$_{saline}$ mice that were normalized in db/db$_{GLP\text{-}1}$ mice (Figure 6B). There were no differences in left atrial resting membrane potential, AP upstroke velocity (V_{max}), or AP overshoot between treatment groups (Figures 6C to 6E). Consistent with the data in intact atrial preparations, left atrial APD was prolonged throughout repolarization in db/db$_{saline}$ mice and normalized in db/db$_{GLP\text{-}1}$ mice (Figure 6F to 6I). Very similar effects of GLP-1 on AP morphology were observed in isolated right atrial myocytes (Supplemental Figure 5).

In addition, variability in APD was assessed using Poincaré plot analysis (Supplemental Figures 6A and 6B). Quantification of SDs (SD1 and SD2) of Poincaré plots demonstrate that APD heterogeneity was increased in db/db$_{saline}$ mice throughout repolarization compared to wild-type mice and largely normalized in db/db$_{GLP\text{-}1}$ mice (Supplemental Figures 6C to 6J).

Consistent with the absence of differences in AP upstroke velocity or V_{max}, there were no differences in peak I_{Na} density (Supplemental Figures 7A and 7B) or I_{Na} steady-state activation kinetics (Supplemental Figure 7C, Supplemental Table 6) between treatment groups. However, the I_{Na} steady-state inactivation

FIGURE 4 Effects of Chronic Liraglutide Treatment on P-Wave Duration in db/db Mice

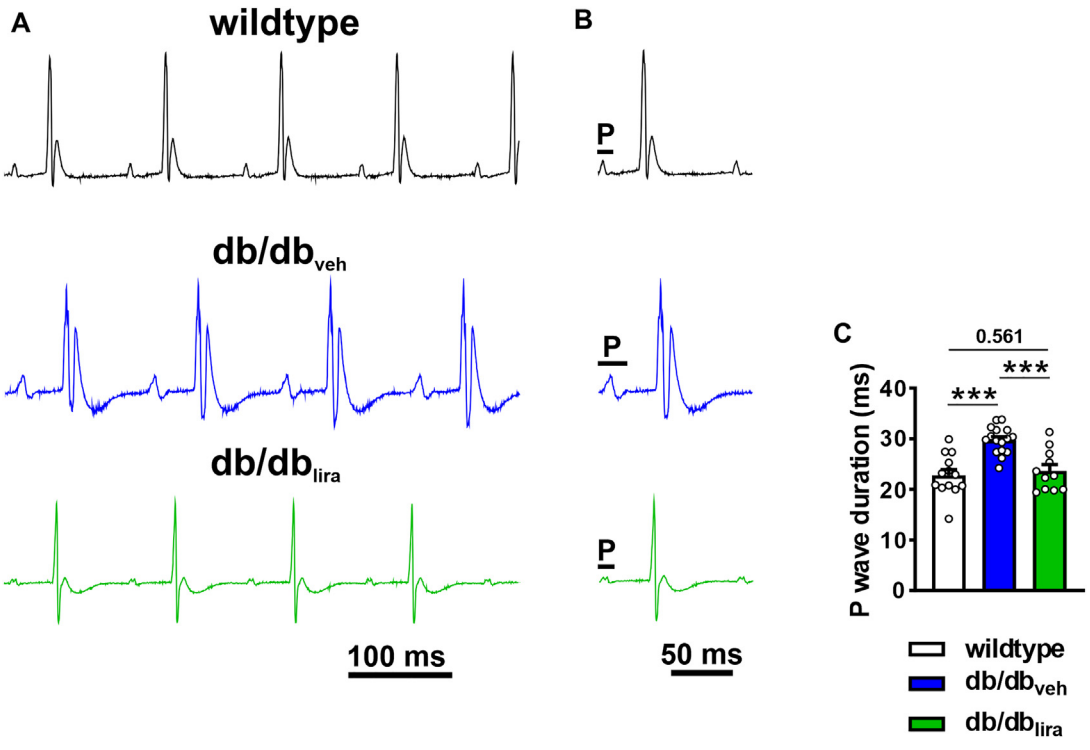

(A) Representative surface ECGs in anesthetized wild-type, db/db$_{veh}$, and db/db$_{lira}$ mice. **(B)** Magnified ECGs in wild-type, db/db$_{veh}$, and db/db$_{lira}$ mice illustrating differences in P-wave duration. **(C)** Summary of P-wave duration in wild-type (n = 13), db/db$_{veh}$ (n = 16), and db/db$_{lira}$ (n = 11) mice. Data analyzed by one-way analysis of variance with Holm-Sidak post hoc test. Refer to Supplemental Table 5 for additional ECG analysis. ***$P < 0.001$. Abbreviations as in **Figures 1 and 3**.

curve was shifted to more positive membrane potentials in db/db$_{saline}$ right atrial myocytes compared to wild-type mice and normalized in db/db$_{GLP\text{-}1}$ myocytes (Supplemental Figure 7D, Supplemental Table 6). This resulted in a larger I_{Na} window current in db/db$_{saline}$ atrial myocytes, which was normalized in db/db$_{GLP\text{-}1}$ atrial myocytes (Supplemental Figures 7E and 7F).

Total K^+ current (I_K) was measured with and without a prepulse to −40 mV to inactivate I_{to} in left atrial myocytes from wild-type, db/db$_{saline}$, and db/db$_{GLP\text{-}1}$ mice (**Figure 7A**). I_K current-voltage relationships measuring peak outward I_K demonstrate that outward I_K was reduced in db/db$_{saline}$ left atrial myocytes and significantly improved in, db/db$_{GLP\text{-}1}$ left atrial myocytes before (**Figures 7B and 7C**) and after (**Figures 7D and 7E**) the inactivating prepulse. The difference current between the I_K recordings with and without the prepulse is a measure of I_{to} (**Figure 8A**). I_{to} was reduced in left atrial myocytes from db/db$_{saline}$ mice compared with wild-type mice and normalized in db/db$_{GLP\text{-}1}$ left atrial myocytes (**Figure 8B**). In addition, I_{Kur} was measured as the 4-aminopyridine (4-AP) (100 μmol/L)-sensitive component of I_K in left atrial myocytes from wild-type, db/db$_{saline}$, and db/db$_{GLP\text{-}1}$ mice (**Figure 8C**). The 4-AP-sensitive I_{Kur} was reduced in left atrial db/db$_{saline}$ myocytes compared with wild-type myocytes and normalized in left atrial db/db$_{GLP\text{-}1}$ myocytes (**Figure 8D**). Similar changes in repolarizing K^+ currents were observed in right atrial myocytes from GLP-1-treated db/db mice (Supplemental Figure 8). Specifically, right atrial I_{to} was reduced in db/db$_{saline}$ mice compared with wild-type mice and significantly improved in db/db$_{GLP\text{-}1}$ mice (Supplemental Figures 9A and 9B). Right atrial 4-AP-sensitive I_{Kur} was also reduced in db/db$_{saline}$ mice compared with in wild-type mice and normalized in db/db$_{GLP\text{-}1}$ mice (Supplemental Figures 9C and 9D).

Expression of *Kcnd2* (encodes $K_V4.2$), *Kcnd3* (encodes $K_V4.3$), and *Kcnip2* (encodes KChIP2) were each reduced in the left atrium of db/db$_{saline}$ mice

FIGURE 5 **Effects of Chronic GLP-1 on Atrial Conduction and Atrial Optical AP Morphology in db/db Hearts**

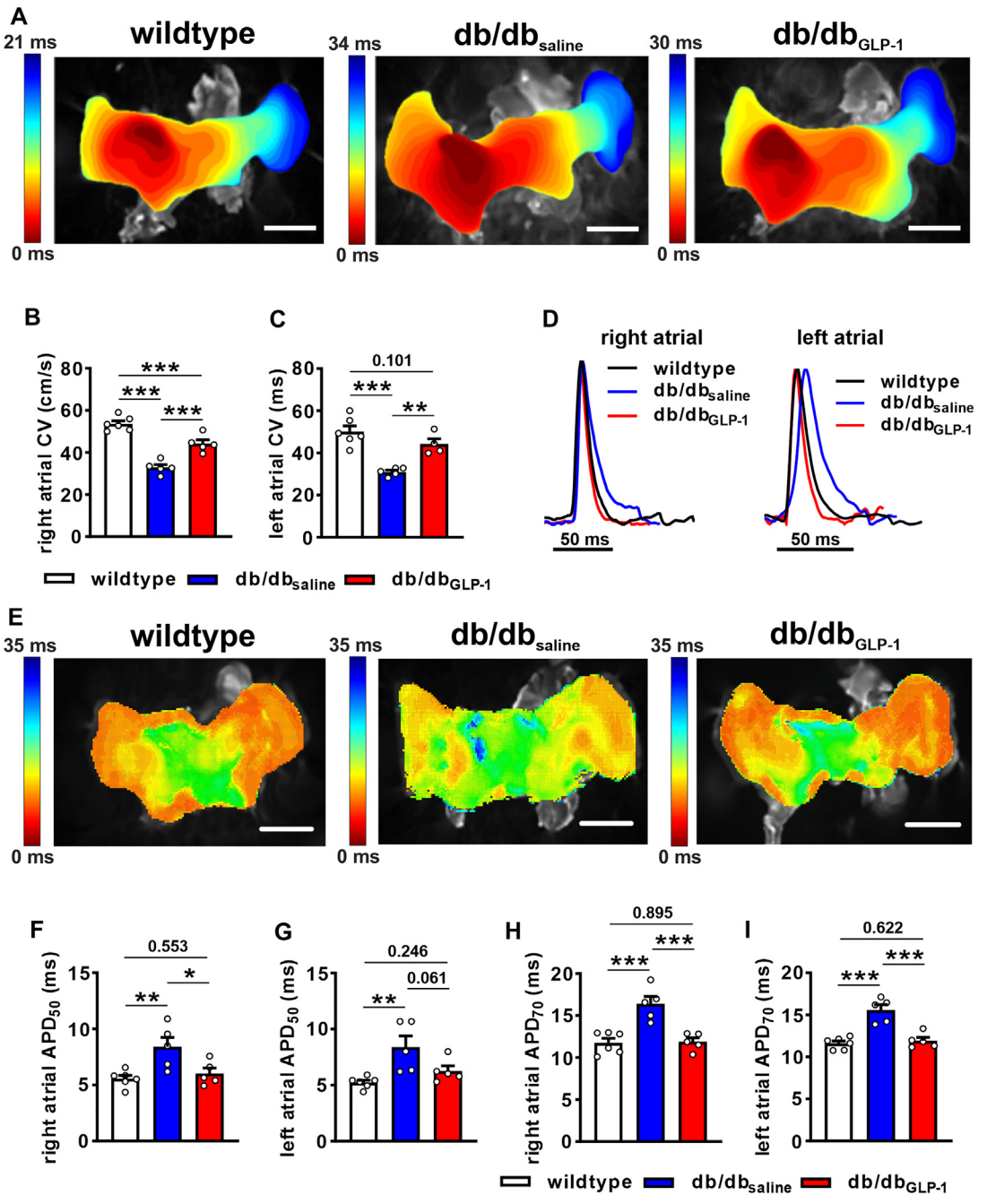

(A) Representative activation maps in isolated atrial preparations from wild-type, db/db_{saline}, and db/$db_{GLP\text{-}1}$ mice paced at 8 Hz. Right atrial appendage is on the **left side of the image**. Color scale indicates total conduction time across the preparation. Bars = 2 mm. **(B, C)** Summary of right atrial **(B)** and left atrial **(C)** conduction velocity (CV) in wild-type, db/db_{saline}, and db/$db_{GLP\text{-}1}$ mice. **(D)** Representative right atrial and left atrial optical action potentials (APs) in isolated atrial preparations from wild-type, db/db_{saline}, and db/$db_{GLP\text{-}1}$ mice. **(E)** Representative action potential duration maps at 50% repolarization time (APD_{50}) in atrial preparations from wild-type, db/db_{saline}, and db/$db_{GLP\text{-}1}$ mice. Bars = 2 mm. **(F, G)** Summary of right **(F)** and left **(G)** atrial APD_{50} in atrial preparations from wild-type, db/db_{saline}, and db/$db_{GLP\text{-}1}$ mice. **(H, I)** Summary of right **(H)** and left **(I)** atrial APD_{70} in atrial preparations from wild-type, db/db_{saline}, and db/$db_{GLP\text{-}1}$ mice. Summary data analyzed by one-way analysis of variance with Holm-Sidak post hoc test; n = 5-6 atrial preparations per group. *$P < 0.05$, **$P < 0.01$, ***$P < 0.001$. Abbreviations as in Figure 1.

compared with wild-type mice and remained reduced compared to wild-type in db/db_{GLP-1} left atria (Supplemental Figures 10A to 10C). Expression of *Kcna5* (encodes $K_V1.5$) was not different between treatment groups (Supplemental Figure 10D). Protein expression of $K_V4.2$ showed a trend ($P = 0.055$) toward reduction in the left atrium of db/db_{saline} mice and was not affected by GLP-1 treatment (Supplemental Figure 10E). Protein expression of $K_V4.3$, KChIP2, and $K_V1.5$ was not different among groups (Supplemental Figures 10F to 10H).

EFFECTS OF ACUTE GLP-1 ON ATRIAL MYOCYTE ACTION POTENTIAL MORPHOLOGY IN DB/DB MICE. The effects of acute GLP-1 (100 nmol/L) application on isolated atrial myocytes from untreated db/db mice were also measured to determine whether this would mimic the effects of chronic GLP-1 treatment described herein. In these experiments, GLP-1 was superfused on isolated atrial myocytes for 5-10 minutes. Acute GLP-1 application had no effects on atrial AP morphology in isolated db/db atrial myocytes (Supplemental Figure 11).

EFFECTS OF CHRONIC GLP-1 ON ATRIAL FIBROSIS IN DB/DB MICE. Interstitial fibrosis at study endpoints was increased in the right and left atria of db/db_{saline} mice and this was significantly attenuated in db/db_{GLP-1} mice (**Figures 9A to 9D**). The progression of fibrosis was also assessed in the left atrium in db/db mice (Supplemental Figure 12). These data demonstrate that left atrial fibrosis was also increased at 12-14 weeks of age (ie, the time point at which GLP-1 or saline infusions began) in db/db mice and tended to be further increased by the study endpoint. Expression of *Col1a* (encodes collagen type I) and *Col3a* (encodes collagen type III) was increased in the left atrium of db/db_{saline} mice compared to wild-type mice and normalized in db/db_{GLP-1} left atria (**Figures 9E and 9F**).

DISCUSSION

AF is highly prevalent in patients with T2DM where it substantially worsens morbidity and mortality.[2,4,5] Consistent with this, the present study, as well as previous studies,[11] show that the db/db mouse model of T2DM is highly susceptible to pacing-induced AF caused by impaired atrial electrical conduction in association with electrical and structural remodeling of the atria. Although some clinical studies have suggested that antidiabetic drugs such as GLP-1R agonists may protect against AF in T2DM,[19] this is very poorly understood. Accordingly, this was investigated in the present study. Strikingly, chronic treatment of db/db mice with GLP-1 (continuous infusion by osmotic pump) reduced susceptibility to AF. Furthermore, AF durations were shorter on average in GLP-1-treated db/db mice, indicating a less severe AF burden. Protection against AF in GLP-1-treated db/db mice occurred in association with improvements in atrial conduction as indicated by shorter P-wave durations in vivo and faster atrial conduction velocities in isolated atrial preparations compared to saline-treated db/db mice. Importantly, treatment of db/db mice with the long-acting GLP-1R analogue liraglutide, using a clinically relevant dose and treatment approach (daily subcutaneous injections), also reduced AF burden. Specifically, liraglutide-treated db/db mice exhibited intermediate levels of AF susceptibility and on average had shorter AF durations. Liraglutide also reduced AERP and shortened P-wave duration to wild-type levels, indicating a normalization of atrial conduction in db/db mice. The intermediate effect of liraglutide compared to GLP-1 on AF susceptibility may be related to dosing and route of delivery as GLP-1 was delivered continuously by osmotic pump whereas liraglutide was delivered by once-daily subcutaneous injection. Overall, the present study demonstrates that GLP-1 (and related GLP-1R agonists) can potently protect against AF and preserve atrial conduction in db/db mice.

db/db mice also exhibited evidence of SAN dysfunction (ie, reduced heart rate, increased cSNRT), which is common in association with AF.[28,29] Previous studies have also demonstrated SAN dysfunction in db/db mice.[30] Overall, GLP-1 did not prevent these changes in SAN function. We did not observe substantial changes in atrial or ventricular size or ventricular function in db/db mice by echocardiography, which is consistent with our previous study.[11] The present study shows that echocardiography measures were also not significantly affected by GLP-1. On the other hand, patch-clamp studies demonstrated increased cell capacitance in db/db_{saline} mice that were normalized in db/db_{GLP-1} mice. This suggests that db/db mice may exhibit atrial myocyte hypertrophy, which was prevented by GLP-1.

Whereas atrial electrophysiology was substantially altered in db/db mice and potently affected by GLP-1, ventricular ECG intervals were not markedly altered in db/db mice and were not significantly affected by GLP-1 or liraglutide. GLP-1R is highly expressed in the atria, possibly at levels higher than in the ventricles,[13] suggesting that GLP-1 may act, at least in part, via direct effects in the atria. Consistent with this, blood pressure was not different in db/db mice and not

FIGURE 6 Effects of Chronic GLP-1 on AP Morphology in Isolated Left Atrial Myocytes in db/db Mice

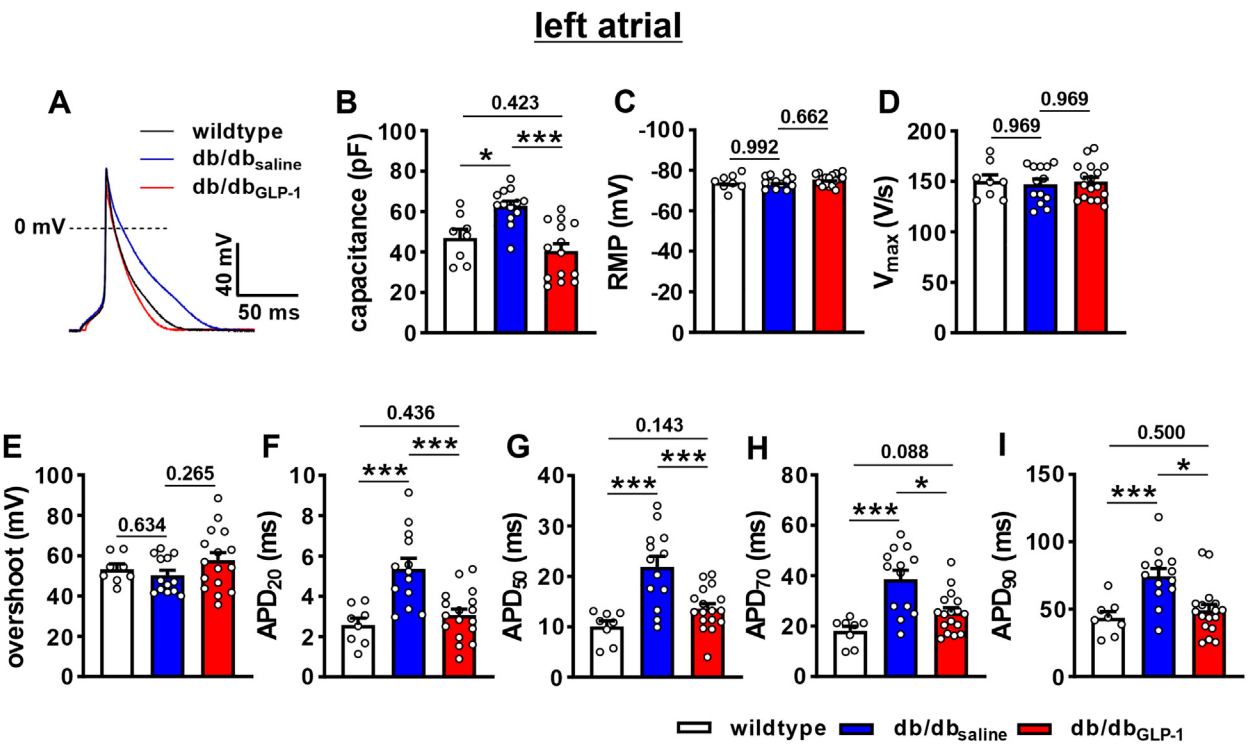

(A) Representative stimulated APs in left atrial myocytes isolated from wild-type, db/db$_{saline}$, and db/db$_{GLP-1}$ mice. **(B to I)** Summary data for cell capacitance **(B),** resting membrane potential (RMP) **(C),** AP upstroke velocity (V_{max}) **(D),** overshoot **(E),** APD_{20} **(F),** APD_{50} **(G),** APD_{70} **(H),** and APD_{90} **(I)** in isolated left atrial myocytes from wild-type, db/db$_{saline}$, and db/db$_{GLP-1}$ mice. Data analyzed by one-way analysis of variance with Holm-Sidak post hoc test; n = 8 myocytes from 2 mice for wild type, 13 myocytes from 5 mice for db/db$_{saline}$, and 17 cells from 9 mice for db/db$_{GLP-1}$. *$P < 0.05$, ***$P < 0.001$. Abbreviations as in Figures 1 and 5.

affected by GLP-1. There were also no effects of GLP-1 or liraglutide on plasma insulin levels, which were similarly elevated in saline- and drug-treated db/db mice. On the other hand, GLP-1 and liraglutide caused some improvement in blood glucose levels in db/db mice, although not to wild-type levels. This is consistent with previous studies showing that liraglutide partially improves glucose tolerance in db/db mice.[31,32] Thus, it is possible that a partial reduction in the level of hyperglycemia could contribute to the improvements in atrial electrophysiology elicited by GLP-1R agonists via indirect effects. It is important to note, however, that the relationship between AF prevalence and glycemic control in patients with diabetes remains unresolved with some studies suggesting worsening AF with poor glycemic control and others finding no relationship.[2,4,6,33] Further studies will be needed to delineate direct and indirect effects of GLP-1R agonists on atrial electrophysiology.

Several factors can affect atrial conduction velocity including AP upstroke velocity caused by I_{Na}, gap junctions, and fibrosis.[7] We observed no differences in atrial AP upstroke velocity or atrial peak I_{Na} in db/db mice and neither of these were altered by GLP-1 treatment. We have also previously shown that messenger RNA expression of major atrial connexins (Cx40 and Cx43) is not altered in db/db mice.[11] In contrast, db/db mice exhibited fibrosis in the right and left atria in association with increases in expression of collagen type I and collagen type III. Atrial fibrosis was significantly lower in db/db atria after GLP-1 treatment. Atrial fibrosis was also increased at 12-14 weeks of age in db/db mice (which corresponds to the time point at which GLP-1 treatment began) and tended to increase further at time points corresponding to study endpoints when functional studies were conducted. This suggests that GLP-1 acts to prevent further fibrosis from developing but may also partially reverse fibrosis. Consistent with this, GLP-1 also normalized atrial collagen gene expression in db/db mice. These data indicate that changes in fibrosis are critically involved in the

FIGURE 7 Effects of Chronic GLP-1 on K^+ Currents in Isolated Left Atrial Myocytes in db/db Mice

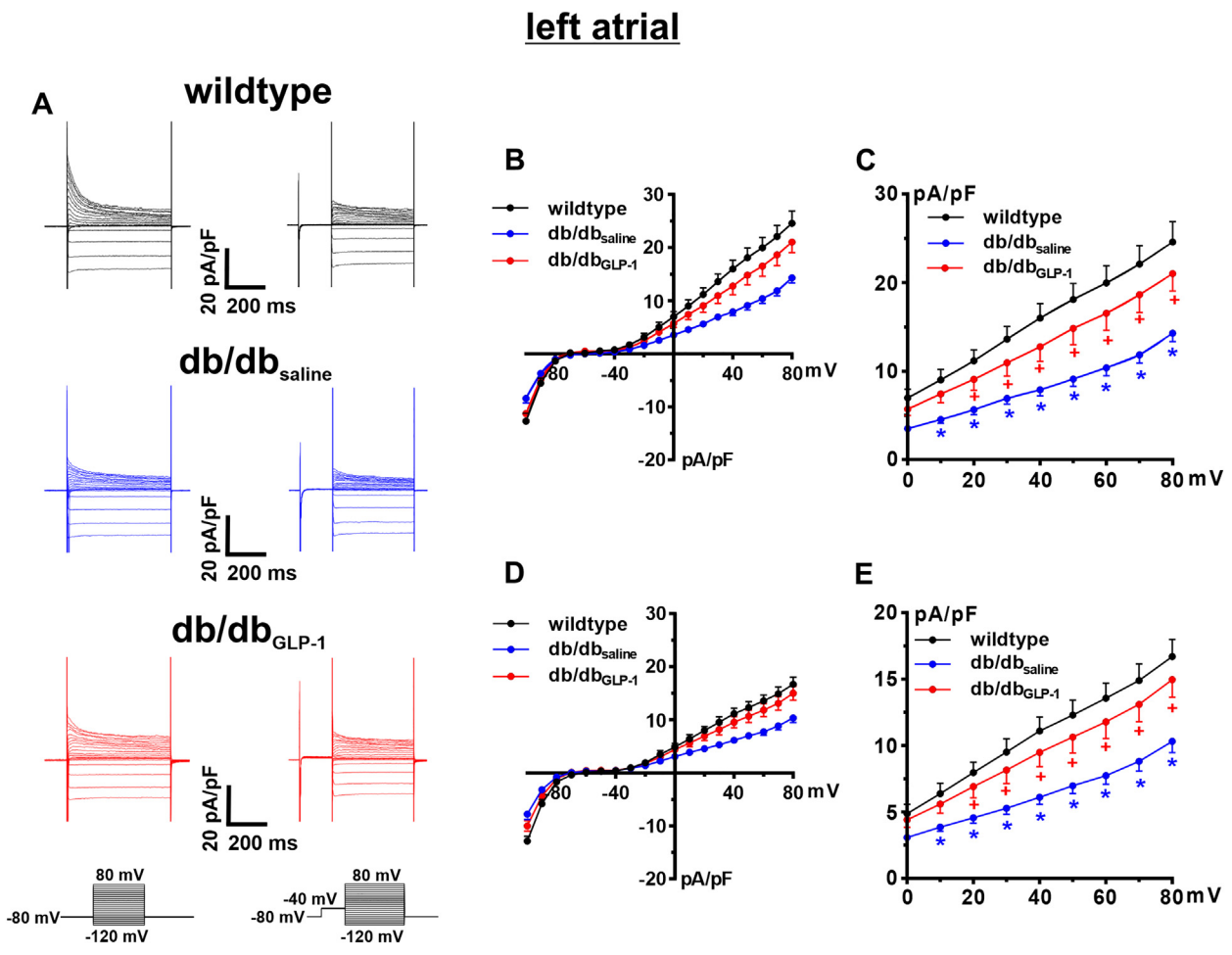

(A) Representative K^+ current (I_K) recordings for total I_K **(left)** and I_K after an inactivating prepulse to −40 mV **(right)** in left atrial myocytes isolated from wild-type, db/db_{saline}, and db/db_{GLP-1} mice. Voltage clamp protocols shown below recordings. **(B)** I_K current-voltage (IV) curves measured at the peak of the total I_K recordings. **(C)** I_K IV curves (same data as **B**) showing repolarizing I_K at membrane potentials positive to 0 mV. **(D)** I_K IV curves measured at the peak of the I_K recordings after an inactivating prepulse. **(E)** I_K IV curves after an inactivating prepulse (same data as **D**) showing I_K at membrane potentials positive to 0 mV. $^*P < 0.05$ vs wild type, $^+P < 0.05$ vs db/db_{saline} by mixed-effects analysis of variance with Holm-Sidak post hoc test; n = 7 myocytes from 2 mice for wild type, 11 myocytes from 3 mice for db/db_{saline}, and 15 myocytes from 5 mice for db/db_{GLP-1}. Statistical symbols shown only on **C** and **E** for clarity. Abbreviations as in Figure 1.

impairments in atrial conduction velocity in db/db mice and their prevention following treatment with GLP-1. GLP-1 could directly affect fibroblast function; however, it is also possible that GLP-1 could affect inflammatory signaling, which could then have an impact on fibroblast activation and profibrotic signaling. Inflammation has been linked to fibrosis and atrial arrhythmias in prior studies.[34] These possibilities will be explored in future studies.

Impaired conduction caused by atrial fibrosis can create a substrate for re-entry, which favors the occurrence and maintenance of AF.[7,35] Consistent with the findings in our study, previous studies have shown that GLP-1R agonists or dipeptidyl peptidase 4 inhibitors (which prevent the hydrolysis of GLP-1) can have antifibrotic effects in the heart in nondiabetic mouse models of disease.[36-38]

In addition, we observed substantial heterogeneity in APD during repolarization in db/db mice, which was prevented by GLP-1 treatment. Increased heterogeneity in repolarization can also lead to re-entry;[39] therefore, the ability of GLP-1 to protect

FIGURE 8 Effects of Chronic GLP-1 on I_{to} and 4-AP-sensitive I_{Kur} in Isolated Left Atrial Myocytes in db/db Mice

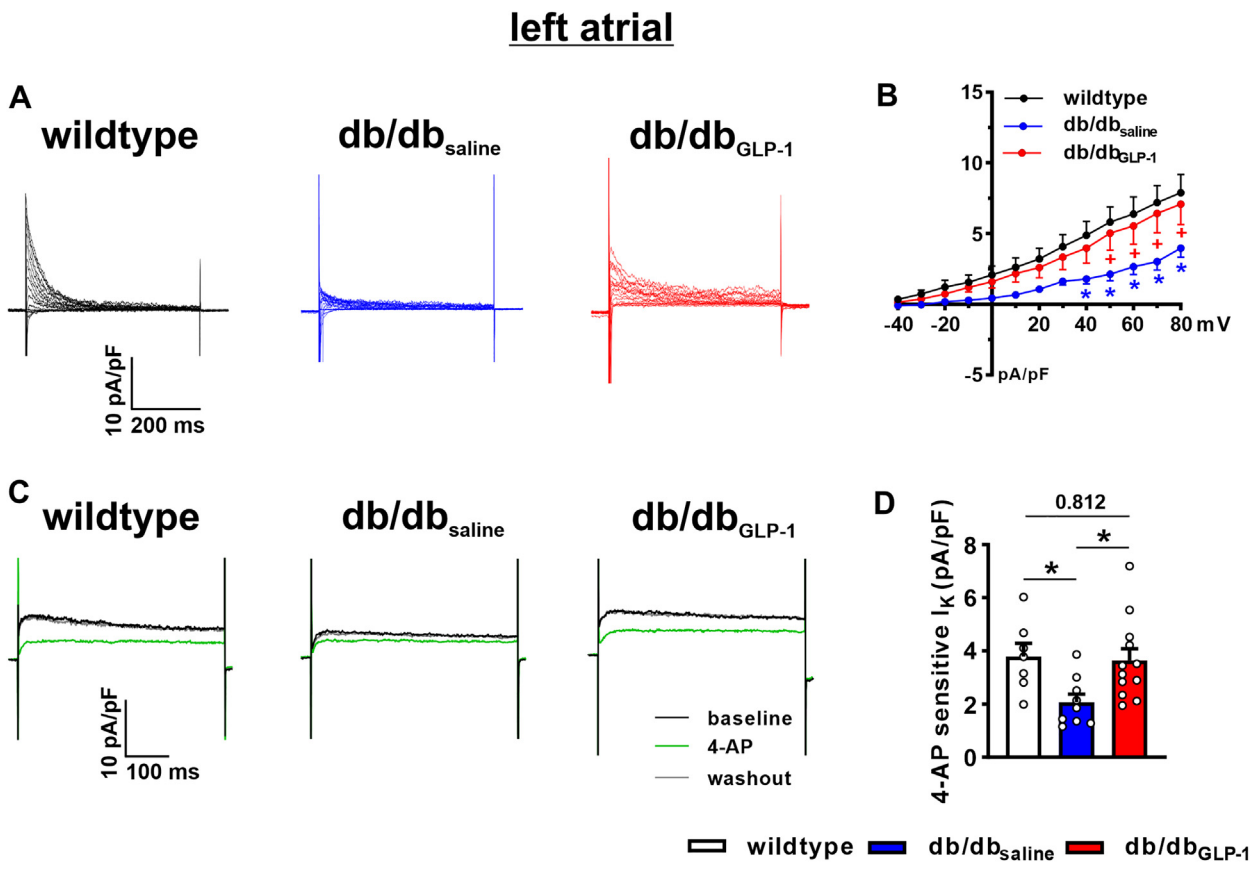

(A) Representative transient outward K^+ current (I_{to}) recordings in isolated left atrial myocytes from wild-type, db/db_{saline}, and db/db_{GLP-1} mice generated by digitally subtracting the I_K recordings with and without a prepulse as seen in Figure 7. **(B)** I_{to} IV curves measured as the difference current between I_K recordings with and without a prepulse as shown in Figure 7. *$P < 0.05$ vs wild-type mice; $^{+}P < 0.05$ vs db/db_{GLP-1} mice by mixed effects analysis of variance with Holm-Sidak post hoc test; n = 7 myocytes from 2 mice for wild type, 11 myocytes from 3 mice for db/db_{saline}, and 15 myocytes from 5 mice for db/db_{GLP-1}. **(C)** Representative I_K recordings at +30 mV showing the effects of 4-aminopyridine (4-AP) (100 μmol/L), which inhibits $K_V1.5$-mediated I_{Kur}, in isolated left atrial myocytes from wild-type, db/db_{saline}, and db/db_{GLP-1} mice. **(D)** Summary of the amplitude of 4-AP–sensitive I_K in isolated left atrial myocytes from wild-type, db/db_{saline}, and db/db_{GLP-1} mice. Data analyzed by one-way analysis of variance with Holm-Sidak post hoc test; n = 7 myocytes from 2 mice for wild type, 9 myocytes from 3 mice for db/db_{saline}, and 12 myocytes from 5 mice for db/db_{GLP-1}. I_{Kur} = ultra-rapid delayed rectifier K^+ current; other abbreviations as in Figures 1 and 7.

against this heterogeneity in APD may also contribute to the protective effects of GLP-1 against AF in db/db mice.

Consistent with previous studies,[11] we also observed increases in atrial APD in db/db mice. Increased APD was evident from optical mapping studies in intact atrial preparations and from patch-clamp studies in isolated atrial myocytes and coincided with increases in AERP in vivo. Increased atrial APD occurred because of reductions in repolarizing I_{to} and I_{Kur}. Although peak I_{Na} was not altered in db/db atrial myocytes, the I_{Na} steady-state inactivation curve was shifted to more positive membrane potentials resulting in a larger I_{Na} window current that could also contribute to AP prolongation. Chronic GLP-1 treatment normalized APD, prevented the reductions in I_{to} and I_{Kur}, and normalized I_{Na} steady-state inactivation in db/db atrial myocytes. In addition to fibrosis, prolongation of APD could also contribute to the slowing of atrial conduction, particularly at high heart rates, while also increasing the potential for conduction block.[40,41] Each of these could further contribute to a substrate for re-entry and AF in db/db mice. In addition, AP prolongation could increase the likelihood of early afterdepolarizations, which could trigger AF occurrence.

FIGURE 9 Effects of Chronic GLP-1 on Atrial Fibrosis in db/db Mice

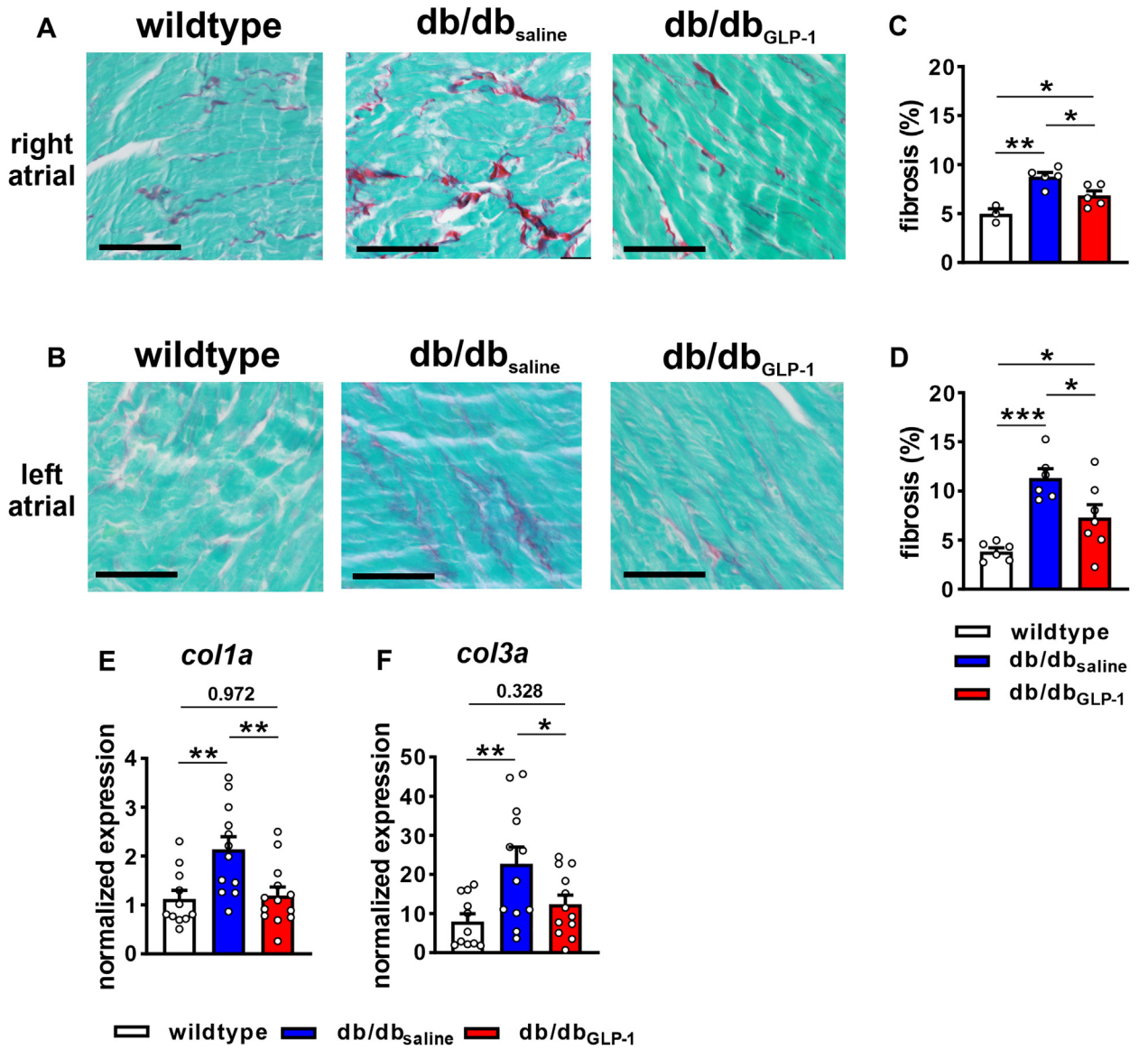

(A, B) Representative images showing patterns of interstitial fibrosis (red staining) in right **(A)** and left **(B)** atria of wild-type, db/db_{saline}, and db/db_{GLP-1} mice. Bars = 50 μm. **(C,D)** Summary of right **(C)** and left **(D)** atrial fibrosis. Data analyzed by one-way analysis of variance with Holm-Sidak post hoc test. For right atrium, n = 3 wild-type, 5 db/db_{saline}, and 5 db/db_{GLP-1} mice. For left atrium, n = 6 wild-type, 6 db/db_{saline}, and 7 db/db_{GLP-1} mice. **(E-F)** Messenger RNA expression of *Col1a* **(E)** and *Col3a* **(F)** in the left atrium in wild-type, db/db_{saline}, and db/db_{GLP-1} mice. Data analyzed by one-way analysis of variance with Holm-Sidak post hoc test, n = 11 wild-type, 12, db/db_{saline}, and 13 db/db_{GLP-1} mice. *$P < 0.05$, **$P < 0.01$, ***$P < 0.001$. Abbreviations as in Figure 1.

Thus, the prevention of increases in APD by GLP-1 is likely centrally involved in the improvements in atrial conduction and protection against AF in db/db mice treated with GLP-1.

In agreement with previous studies,[11] I_{to} was reduced in db/db atria in association with reduced expression of *Kcnd2*, *Kcnd3,* and *Kcnip2* and lower protein expression of $K_v4.2$. Interestingly, these changes were not prevented by GLP-1 treatment. GLP-1 treatment also had no effects on the protein expression of $K_v4.3$ or KChIP2. Furthermore, there were no changes in expression of *Kcna5* or $K_V1.5$

protein in db/db mice before or after GLP-1 treatment. Thus, GLP-1 was able to increase I_{to} and I_{Kur} current density independently of changes in ion channel gene or protein expression. As noted, cell capacitance was increased in db/db atrial myocytes (indicating atrial hypertrophy) and this was prevented by GLP-1 treatment; therefore, the improvements in I_{to} and I_{Kur} density in db/db_{GLP-1} mice may be associated with these differences in cell capacitance and the prevention of atrial myocyte hypertrophy. The mechanisms by which GLP-1 improves atrial K^+ currents in db/db mice will be studied further in future investigations.

Acute application of GLP-1 had no effects on AP morphology in isolated atrial myocytes from db/db mice. It is also reasonable to infer that an acute exposure to GLP-1 treatment would have minimal affects, if any, on atrial fibrosis. Together, these data indicate that GLP-1 must be delivered chronically to achieve protection against atrial electrical remodeling (ie, changes in AP morphology and associated ionic currents) and structural remodeling (ie, fibrosis) in db/db mice.

STUDY LIMITATIONS. The present study was conducted in mice, which exhibit some differences in repolarizing K^+ currents compared to humans.[42] Specifically, the rapid and slow delayed rectifier K^+ currents (I_{Kr} and I_{Ks}) do not play a major functional role in mouse atria. However, I_{to} and I_{Kur}, which are centrally involved in the changes in AP morphology in db/db mice before and after GLP-1 treatment, are critical in the atria of mice and humans, suggesting the effects identified in the present study will be relevant to humans. Further studies to determine optimal doses and duration of treatment with specific GLP-1R agonists to optimize effects on atrial electrophysiology while also ensuring appropriate glycemic control are warranted.

CONCLUSIONS

The present study demonstrates that chronic treatment of type 2 diabetic db/db mice with GLP-1 protects against AF by preventing impairments in atrial conduction, atrial electrical remodeling, and atrial fibrosis. These findings suggest that GLP-1R agonists could protect against AF in human patients with T2DM. Given the wide use of GLP-1R agonists for the treatment of T2DM, the effects of these compounds on AF in these patients should be further studied.

FUNDING SUPPORT AND AUTHOR DISCLOSURES

Dr Bohne has received a University of Calgary Graduate Scholarship. Dr Jansen has received a Killam Postdoctoral Fellowship. Dr Dorey has received a Canadian Institutes of Health Research Doctoral Research Award. Dr Jamieson has received a Libin Cardiovascular Institute Postdoctoral Fellowship. Dr Rose has received support from the Canadian Institutes of Health Research (grants PJT180474 and PJT166105). All other authors have reported that they have no relationships relevant to the contents of this paper to disclose.

ADDRESS FOR CORRESPONDENCE: Dr Robert A. Rose, Libin Cardiovascular Institute, Cumming School of Medicine, University of Calgary, GAC66, Health Research Innovation Centre, 3280 Hospital Drive NW, Calgary, Alberta T2N 4Z6, Canada. E-mail: robert.rose@ucalgary.ca.

PERSPECTIVES

COMPETENCY IN MEDICAL KNOWLEDGE: Atrial fibrillation is highly prevalent in patients with T2DM. Furthermore, patients with T2DM that develop AF experience worse outcomes including increased mortality. GLP-1R agonists are used to treat patients with T2DM; however, their effects on atrial remodeling and AF are unclear. We demonstrate that GLP-1 and the GLP-1 analogue liraglutide protect against AF in type 2 diabetic mice by preventing electrical and structural remodeling in the atria.

TRANSLATIONAL OUTLOOK: This study identifies GLP-1 and the related GLP-1 analogue liraglutide as a potential approach for treating or preventing AF in a mouse model of T2DM. Further studies will be required to translate these finding to human patients with T2DM to reduce the influences of AF in this patient population.

REFERENCES

1. Staerk L, Sherer JA, Ko D, Benjamin EJ, Helm RH. Atrial fibrillation: epidemiology, pathophysiology, and clinical outcomes. *Circ Res*. 2017;120(9):1501–1517.

2. Bohne LJ, Johnson D, Rose RA, Wilton SB, Gillis AM. The association between diabetes mellitus and atrial fibrillation: clinical and mechanistic insights. *Front Physiol*. 2019;10:135.

3. Kahn SE, Cooper ME, Del Prato S. Pathophysiology and treatment of type 2 diabetes: perspectives on the past, present, and future. *Lancet*. 2014;383(9922):1068–1083.

4. Bell DSH, Goncalves E. Atrial fibrillation and type 2 diabetes: prevalence, etiology, pathophysiology and effect of anti-diabetic therapies. *Diabetes Obes Metab*. 2019;21(2):210–217.

5. Kornej J, Borschel CS, Benjamin EJ, Schnabel RB. Epidemiology of atrial fibrillation in

the 21st century: novel methods and new insights. *Circ Res*. 2020;127(1):4–20.

6. Andrade J, Khairy P, Dobrev D, Nattel S. The clinical profile and pathophysiology of atrial fibrillation: relationships among clinical features, epidemiology, and mechanisms. *Circ Res*. 2014;114(9):1453–1468.

7. Jansen HJ, Bohne LJ, Gillis AM, Rose RA. Atrial remodeling and atrial fibrillation in acquired forms of cardiovascular disease. *Heart Rhythm O2*. 2020;1(2):147–159.

8. Aguilar M, Rose RA, Takawale A, Nattel S, Reilly S. New aspects of endocrine control of atrial fibrillation and possibilities for clinical translation. *Cardiovasc Res*. 2021;117(7):1645–1661.

9. Heijman J, Voigt N, Nattel S, Dobrev D. Cellular and molecular electrophysiology of atrial fibrillation initiation, maintenance, and progression. *Circ Res*. 2014;114(9):1483–1499.

10. Bartos DC, Grandi E, Ripplinger CM. Ion channels in the heart. *Compr Physiol*. 2015;5(3):1423–1464.

11. Bohne LJ, Jansen HJ, Daniel I, et al. Electrical and structural remodeling contribute to atrial fibrillation in type 2 diabetic db/db mice. *Heart Rhythm*. 2021;18(1):118–129.

12. Ussher JR, Drucker DJ. Cardiovascular biology of the incretin system. *Endocr Rev*. 2012;33(2):187–215.

13. Ussher JR, Drucker DJ. Cardiovascular actions of incretin-based therapies. *Circ Res*. 2014;114(11):1788–1803.

14. Ussher JR, Greenwell AA, Nguyen MA, Mulvihill EE. Cardiovascular effects of incretin-based therapies: integrating mechanisms with cardiovascular outcome trials. *Diabetes*. 2022;71(2):173–183.

15. Nauck MA, Meier JJ, Cavender MA, Abd El Aziz M, Drucker DJ. Cardiovascular actions and clinical outcomes with glucagon-like peptide-1 receptor agonists and dipeptidyl peptidase-4 inhibitors. *Circulation*. 2017;136(9):849–870.

16. Marso SP, Daniels GH, Brown-Frandsen K, et al. LEADER Steering Committee and Trial Investigators. Liraglutide and cardiovascular outcomes in type 2 diabetes. *N Engl J Med*. 2016;375(4):311–322.

17. Baggio LL, Yusta B, Mulvihill EE, et al. GLP-1 receptor expression within the human heart. *Endocrinology*. 2018;159(4):1570–1584.

18. Drucker DJ, Dritselis A, Kirkpatrick P. *Liraglutide. Nat Rev Drug Discov*. 2010;9(4):267–268.

19. Shi W, Zhang W, Zhang D, et al. Comparison of the effect of glucose-lowering agents on the risk of atrial fibrillation: a network meta-analysis. *Heart Rhythm*. 2021;18(7):1090–1096.

20. Nakamura H, Niwano S, Niwano H, et al. Liraglutide suppresses atrial electrophysiological changes. *Heart Vessels*. 2019;34(8):1389–1393.

21. Hsueh W, Abel ED, Breslow JL, et al. Recipes for creating animal models of diabetic cardiovascular disease. *Circ Res*. 2007;100(10):1415–1427.

22. Zhang J, Tokui Y, Yamagata K, et al. Continuous stimulation of human glucagon-like peptide-1 (7-36) amide in a mouse model (NOD) delays onset of autoimmune type 1 diabetes. *Diabetologia*. 2007;50(9):1900–1909.

23. Nair AB, Jacob S. A simple practice guide for dose conversion between animals and human. *J Basic Clin Pharm*. 2016;7(2):27–31.

24. Polina I, Jansen HJ, Li T, et al. Loss of insulin signaling may contribute to atrial fibrillation and atrial electrical remodeling in type 1 diabetes. *Proc Natl Acad Sci U S A*. 2020;117(14):7990–8000.

25. Jansen HJ, Mackasey M, Moghtadaei M, et al. Distinct patterns of atrial electrical and structural remodeling in angiotensin II mediated atrial fibrillation. *J Mol Cell Cardiol*. 2018;124:12–25.

26. Ripplinger CM, Glukhov AV, Kay MW, et al. Guidelines for assessment of cardiac electrophysiology and arrhythmias in small animals. *Am J Physiol Heart Circ Physiol*. 2022;323(6):H1137–H1166.

27. Jansen HJ, Mackasey M, Moghtadaei M, et al. NPR-C (natriuretic peptide receptor-C) modulates the progression of angiotensin ii-mediated atrial fibrillation and atrial remodeling in mice. *Circ Arrhythm Electrophysiol*. 2019;12(1):e006863.

28. Bukari A, Wali E, Deshmukh A, et al. Prevalence and predictors of atrial arrhythmias in patients with sinus node dysfunction and atrial pacing. *J Interv Card Electrophysiol*. 2018;53(3):365–371.

29. Chang HY, Lin YJ, Lo LW, et al. Sinus node dysfunction in atrial fibrillation patients: the evidence of regional atrial substrate remodelling. *Europace*. 2013;15(2):205–211.

30. Liu Y, Jansen HJ, Krishnaswamy PS, Bogachev O, Rose RA. Impaired regulation of heart rate and sinoatrial node function by the parasympathetic nervous system in type 2 diabetic mice. *Sci Rep*. 2021;11(1):12465.

31. Li Y, Zheng J, Shen Y, et al. Comparative study of liraglutide and insulin glargine on glycemic control and pancreatic beta-cell function in db/db mice. *Med Sci Monit*. 2018;24:3293–3300.

32. Koike M, Saito H, Kohno G, Takubo M, Watanabe K, Ishihara H. Effects of GLP-1RA and SGLT2i, alone or in combination, on mouse models of type 2 diabetes representing different disease stages. *Int J Mol Sci*. 2021;22(21):11463.

33. Benjamin EJ, Levy D, Vaziri SM, D'Agostino RB, Belanger AJ, Wolf PA. Independent risk factors for atrial fibrillation in a population-based cohort. The Framingham Heart Study. *JAMA*. 1994;271(11):840–844.

34. Scott L Jr, Fender AC, Saljic A, et al. NLRP3 inflammasome is a key driver of obesity-induced atrial arrhythmias. *Cardiovasc Res*. 2021;117(7):1746–1759.

35. Nattel S. Molecular and cellular mechanisms of atrial fibrosis in atrial fibrillation. *J Am Coll Cardiol EP*. 2017;3(5):425–435.

36. Wang J, Guo R, Ma X, et al. Liraglutide inhibits AngII-induced cardiac fibroblast proliferation and ECM deposition through regulating miR-21/PTEN/PI3K pathway. *Cell Tissue Bank*. 2023;24(1):125–137.

37. Withaar C, Meems LMG, Markousis-Mavrogenis G, et al. The effects of liraglutide and dapagliflozin on cardiac function and structure in a multi-hit mouse model of heart failure with preserved ejection fraction. *Cardiovasc Res*. 2021;117(9):2108–2124.

38. Banks TE, Rajapaksha M, Zhang LH, Bai F, Wang NP, Zhao ZQ. Suppression of angiotensin II-activated NOX4/NADPH oxidase and mitochondrial dysfunction by preserving glucagon-like peptide-1 attenuates myocardial fibrosis and hypertension. *Eur J Pharmacol*. 2022;927:175048.

39. Avula UMR, Abrams J, Katchman A, et al. Heterogeneity of the action potential duration is required for sustained atrial fibrillation. *JCI Insight*. 2019;5(11):e128765.

40. Carmeliet E. Conduction in cardiac tissue. Historical reflections. *Physiol Rep*. 2019;7(1):e13860.

41. Burton FL, Cobbe SM. Dispersion of ventricular repolarization and refractory period. *Cardiovasc Res*. 2001;50(1):10–23.

42. Nerbonne JM, Kass RS. Molecular physiology of cardiac repolarization. *Physiol Rev*. 2005;85(4):1205–1253.

KEY WORDS arrhythmia, electrophysiology, fibrosis. incretin, ion channels

APPENDIX For a supplemental Methods section, and supplemental figures, and tables, please see the online version of this paper.

Supplemental Appendix

Supplemental Methods

Mice

This study used male and female littermate wild-type and db/db mice between the ages of 16-20 weeks. At this age range db/db mice are obese and display glucose intolerance. The db/db mouse contains an autosomal recessive mutation in the leptin receptor (*Lepr*) gene. Mice homozygous for the mutation display hyperphagia and hyperglycemia. Db/db mice were initially obtained from the Jackson Laboratory (strain C57BL/6J-*Lepr*^{db}) and then bred locally. Homozygous db/db mice and wild-type littermates were used in this study. Animals were fed *ad libitum* and kept on a 12:12 h light-dark cycle. The diabetic phenotype was determined by oral glucose tolerance test.

Oral glucose tolerance test

Blood glucose levels were assessed by oral glucose tolerance test (OGTT). After 6 hours of fasting, mice were administered 50 mg of glucose by oral gavage. Blood samples were taken from the tail vein at regular intervals and blood glucose was measured with a glucometer (StatStrip Xpress®, Nova Biomedical, MA).

Osmotic pump insertion

For chronic GLP-1 studies db/db mice implanted with osmotic mini-pumps (Model 2004, Alzet) containing GLP-1 (7-36 amide). In control experiments db/db mice were implanted with pumps containing saline. GLP-1 was synthesized (Synpeptide Co) with the following amino acid sequence: His-Ala-Glu-Gly-Thr-Phe-Thr-Ser-Asp-Val-Ser-Ser-Tyr-Leu-Glu-Gly-Gln-Ala-Ala-Lys-Glu-Phe-Ile-Ala-Trp-Leu-Val-Lys-Gly-Arg-NH_2. Mice were anesthetized using isoflurane

inhalation (2-3%) and osmotic pumps were inserted subcutaneously via a 1-2 cm mid-scapular incision. Mice were given meloxicam (5 mg/kg) subcutaneously for post-operative analgesia.

Liraglutide treatment

For chronic liraglutide studies db/db mice were given subcutaneous injections of liraglutide or vehicle control once per day at approximately 9 AM each morning. Liraglutide was obtained from Synpeptide Co or from Bachem and had the following sequence: His-Ala-Glu-Gly-Thr-Phe-Thr-Ser-Asp-Val-Ser-Ser-Tyr-Leu-Glu-Gly-Gln-Ala-Ala-Lys(γ-Glupalmitoyl)-Glu-Phe-Ile-Ala-Trp-Leu-Val-Arg-Gly-Arg-Gly. Liraglutide was reconstituted in DMSO (1 mg/mL) and diluted in saline to a 10 μM stock solution. Vehicle consisted of a 3.7% DMSO solution in saline.

Insulin assay

Blood was collected via cardiac puncture from mice fasted for 4-6 hrs in tubes containing 0.04 mL of 7.5% EDTA solution. Whole blood was centrifuged at 1,000 rpm for 10 min to separate plasma, which was collected and frozen at −20 °C until experimental use. Plasma insulin was quantified using a mouse insulin ELISA assay (Mercodia Inc) according to manufacturer's instructions.

Blood pressure

Blood pressure was measured in conscious restrained mice using the CODA tail cuff system (Kent Scientific). Mice underwent 2 days of training prior to measurements. All blood pressure measurements were performed in a quiet dark room at a similar time of day. Data were analyzed using the CODA analysis software.

Echocardiography

Cardiac structure and function were assessed by echocardiography in mice anesthetized by isoflurane inhalation (2%) using a Vevo 3100 ultrasound system (Fujifilm VisualSonics, Canada).

***In vivo* electrophysiology**

A 1.2 French octapolar electrophysiology catheter containing 8 electrodes spaced 0.5 mm apart was used for intracardiac pacing experiments as we have described previously. Inducibility of AF was studied using 3 burst pacing protocols in the mid or high right atrium. The first protocol delivered a train of 45 pulses at a cycle length of 40 ms. After 2 min of rest the second protocol consisting of 80 pulses at a cycle length of 20 ms was applied. Finally, after an additional 2 min of rest, the third protocol consisting of 67 pulses at a cycle length of 20 ms was delivered. Pulse duration was 2 ms and each protocol was delivered 10 times. AF was defined as a rapid and irregular atrial rhythm (fibrillatory baseline in the ECG) with irregular RR intervals lasting at least 1 s on the surface ECG. Effective refractory periods (ERPs) were measured using a S1-S2 protocol where an 8 stimulus drive train (S1) at a fixed cycle length of 100 ms was delivered followed by an extra stimulus (S2) at a progressively shorter cycle length. AERP was defined as the shortest S1-S2 interval resulting in loss of capture of the P wave while AVERP was defined as the shortest S1-S2 interval resulting in a dropped QRS complex for AVERP measurements. Sinoatrial node recovery time (SNRT) was measured by delivering a 12 stimulus drive train at a cycle length of 100 ms. SNRT was defined as the time between the last stimulus in the drive train and the occurrence of the first spontaneous atrial beat (P wave). SNRT was corrected for heart rate (cSNRT) by subtracting the prestimulus RR interval from the measured SNRT. All ECG data were acquired using a Gould ACQ-7700 amplifier and Ponemah Physiology Platform software (Data Sciences International). Body temperature was maintained at 37 °C using a heating pad.

High-resolution optical mapping

To isolate atrial preparations, mice were administered a 0.2 mL intraperitoneal injection of heparin (1,000 IU/mL) to prevent blood clotting and were then anesthetized by isoflurane inhalation and sacrificed by cervical dislocation. Hearts were excised into Krebs solution (37°C) containing (in mM): 118 NaCl, 4.7 KCl, 1.2 KH_2PO_4, 25 $NaHCO_3$, 1 $CaCl_2$, 1 $MgCl_2$, 11 glucose and bubbled with 95% O_2/5% CO_2 to maintain a pH of 7.4. The atria were dissected away from the ventricles and pinned in a dish with the epicardial surface facing upward (toward the imaging equipment). The superior and inferior vena cavae were cut open so that the crista terminalis could be visualized, and the preparation could be pinned out flat with minimal tension.

The atrial preparation was superfused continuously with Krebs solution (37°C) bubbled with 95% O_2/5% CO_2 and allowed to equilibrate for ~10 min. The preparation was then incubated with the voltage sensitive dye RH-237 (15 μM; Biotium) for 15 min without superfusion. After the dye incubation period, superfusion was resumed with blebbistatin (10 μM; Cayman Chemical Company) added to the superfusate to suppress contractile activity and prevent motion artifacts. Experiments were performed in sinus rhythm so that the cycle length (ie, beating rate) of the atrial preparation was free to change as well as in atrial preparations paced at a fixed cycle length of 125 ms (8Hz) in order to study electrical conduction independently of changes in cycle length. The pacing electrode was placed near the opening of the superior vena cava. RH-237-loaded atrial preparations were illuminated with light from the X-Cite Xylis Broad Spectrum LED Illumination System (Excelitas Technologies) and filtered with a 520/35 nm excitation filter (Semrock). Emitted fluorescence was separated by a dichroic mirror (560 nm cutoff; Semrock) and filtered by a 715 nm long-pass emissions filter (Andover Corp.). Recordings were captured using a high-speed CMOS camera (MiCAM03-N256, SciMedia). Data were captured from an optical field of view of 11 x 11 mm at a frame rate of 1,000 frames/s using BrainVision software (BrainVision Inc). The spatial resolution was 42.5 x

42.5 μM for each pixel. Magnification was constant in all experiments and no pixel binning was used.

All optical data were analyzed using custom software written in MATLAB® (MathWorks). Pseudocolor electrical activation maps were generated from measurements of activation time at individual pixels as defined by assessment of dF/dt_{max} and background fluorescence was subtracted in all cases. Local conduction velocity (CV) was quantified specifically in the right atrial myocardium (within the right atrial appendage) and the left atrial myocardium (within the left atrial appendage). Activation times at each pixel from a 7 x 7 pixel array were determined and fit to a plane using the least squares fit method. The direction on this plane that is increasing the fastest represents the direction that is perpendicular to the wave front of electrical propagation and the maximum slope represents the inverse of the speed of conduction in that direction. With a spatial resolution of 42.5 x 42.5 μM per pixel, the area of the 7 x 7 pixel array was 297.5 x 297.5 μM. This approach allows assessment the maximum local CV vectors in the atrial region of interest. Optical APs were assessed by measuring the change in fluorescence as a function of time at individual pixels within the right and left atria.

Isolated of mouse atrial myocytes

Mice were administered a 0.2 mL intraperitoneal injection of heparin (1,000 IU/mL) to prevent blood clotting. Briefly, mice were anaesthetized using isoflurane inhalation and then sacrificed by cervical dislocation. The heart was excised into Tyrode's solution (35ºC) consisting of (in mM): 140 NaCl, 5.4 KCl, 1.2 KH_2PO_4, 1.0 $MgCl_2$, 1.8 $CaCl_2$, 5.55 glucose, and 5 HEPES, with pH adjusted to 7.4 with NaOH. Heparin was added to the Tyrode's solution to prevent blood clotting. The right or left atrial appendage was dissected from the heart, cut into strips and then equilibrated and washed in a 'low Ca^{2+}, Mg^{2+} free' solution containing (in mM): 140 NaCl, 5.4 KCl, 1.2 KH_2PO_4, 0.2 $CaCl_2$, 50 taurine, 18.5 glucose, 5 HEPES and 1 mg/mL bovine serum albumin (BSA), with pH adjusted to 6.9 with NaOH. Next, atrial tissue strips were enzymatically

digested for 30 min in 5 mL of 'low Ca^{2+}, Mg^{2+} free' solution that contained collagenase (type II, Worthington Biochemical Corporation), elastase (Worthington Biochemical Corporation) and protease (type XIV, Sigma Chemical Company). Next, the tissue was transferred to 2.5 mL of modified KB solution containing (in mM): 100 potassium glutamate, 10 potassium aspartate, 25 KCl, 10 KH_2PO_4, 2 $MgSO_4$, 20 taurine, 5 creatine, 0.5 EGTA, 20 glucose, 5 HEPES, and 0.1% BSA, with pH adjusted to 7.2 with KOH. Digested tissue strips were mechanically agitated using a wide-bore pipette. This procedure yielded individual right or left atrial myocytes that were stored in KB solution at room temperature and used for electrophysiology experiments within 6 hours of isolation.

Solutions and electrophysiological protocols

Stimulated action potentials (APs) were recorded using the whole cell patch-clamp technique. Myocytes were superfused with normal Tyrode's solution (22–23 °C) containing (in mM): 140 NaCl, 5 KCl, 1 $MgCl_2$, 1 $CaCl_2$, 10 HEPES, and 5 glucose, with pH adjusted to 7.4 with NaOH. The pipette filling solution contained (in mM): 135 KCl, 0.1 $CaCl_2$, 1 $MgCl_2$, 5 NaCl, 10 EGTA, 4 Mg-ATP, 6.6 Na-phosphocreatine, 0.3 Na-GTP and 10 HEPES, with pH adjusted to 7.2 with KOH. The resting membrane potential was corrected for a liquid junction potential of 4.6 mV.

For recording I_{Na} atrial myocytes were superfused with a modified Tyrode's solution (22–23 °C) containing the following (in mM): 130 CsCl, 5 NaCl, 5.4 TEA-Cl, 1 $MgCl_2$, 1 $CaCl_2$, 10 HEPES, 5.5 glucose, (pH 7.4, adjusted with CsOH). Nitrendipine (10 μM) was added to the superfusate to block $I_{Ca,L}$. The pipette solution for I_{Na} contained (in mM): 120 CsCl, 5 NaCl, 1 $MgCl_2$, 0.2 $CaCl_2$, 10 HEPES, 5 MgATP, 0.3 Na-GTP, 5 BAPTA (pH 7.2, adjusted with CsOH). I_{Na} was recorded using 50 ms voltage clamp steps between −100 and 10 mV from a holding potential of −120 mV.

I_{Na} activation kinetics were determined by calculating chord conductance (G) with the equation $G = I/(V_m - E_{rev})$, where V_m represents the depolarizing voltages and E_{rev} is the reversal potential measured from the current-voltage relationships of $I_{Ca,L}$ or I_{Na}. Maximum conductance (G_{max}) and $V_{1/2}$ of activation ($V_{1/2(act)}$) for $I_{Ca,L}$ and I_{Na} were determined using the following function: $G = [(V_m - V_{rev})][G_{max}][-1/[(1 + \exp((V_m - V_{1/2})/k))+1]]$.

I_{Na} steady-state inactivation kinetics were measured using 500 ms prepulse voltage clamp steps between −120 and −30 mV from a holding potential of −120 mV followed by a 20 ms test pulse to −20 mV. Normalized peak currents were plotted as a function of the prepulse potential and the resulting curve was fitted with the Boltzmann function $h = 1/[1 + \exp[V_{1/2} - V]/k]$. These data were used to measure the voltage at which 50% of channels are inactivated ($V_{1/2(inact)}$).

Total potassium currents (I_K) were recorded in the whole cell configuration of the patch clamp technique using the same Tyrode's solution and pipette solutions used to record APs. To record total potassium currents (no prepulse), cells were held at −80 mV then I_K was recorded using a series of voltage clamp steps (500 ms duration) between −120 and +80 mV in 10 mV increments. To record potassium currents with an inactivating prepulse (to inactivate I_{to}), cells were given a 200 ms repulsed to −40 mV immediately followed by 500 ms voltage clamp steps from −120 to +80 mV from a holding potential of −80 mV. For these recordings with and without a prepulse, I_K was measured at the peak current for each voltage step. I_{to} was calculated as the difference current between the recordings with and without a prepulse. I_{Kur}, as carried by $K_V1.5$ channels, was measured as the component of I_K sensitive to 4-aminopyradine (4-AP; 100 μM). The voltage clamp protocol for measuring I_{Kur} included a prepulse to −40 mV for 200 ms to inactivate I_{to} immediately followed by a 500 ms step to +30 mV before returning to a holding potential of −80 mV. Peak currents at baseline, in the presence of 4-AP, and after washout were measured.

AP duration variability was assessed using Poincaré plot analysis. From these plots the SDs (SD1 and SD2) for APD_{70} were calculated using the following equations: $SD1^2 = 1/2[SD(APD_n - APD_{n+1})]^2$ and $SD2^2=2[SD(APD)]^2 - 1/2[SD(APD_n - APD_{n+1})]$.

Micropipettes were pulled from borosilicate glass (with filament, 1.5 mm OD, 0.75 mm ID, Sutter Instrument Company) using a Flaming/Brown pipette puller (model p-87, Sutter Instrument Company). The resistance of these pipettes was 4–8 MΩ when filled with pipette solution. Micropipettes were positioned using a micromanipulator (Burleigh PCS-5000 system) mounted on the stage of an inverted microscope (Olympus IX71). Seal resistance was 2 – 15 GΩ and access resistances were 5–15 MΩ following rupture of the sarcolemma. Series resistance compensation to 85% using an Axopatch 200B amplifier (Molecular Devices). Data were digitized using a Digidata 1440 and pCLAMP 10 software (Molecular Devices) and stored on computer for analysis. No junction potential corrections were applied in our analyses. All patch-clamp studies were conducted at room temperature.

Quantitative PCR

Quantitative gene expression was measured in the right and left atria. Primers for *Kcnd2* (K_V4.2), *Kcnd3* (K_V4.3), *Kcnip2* (KChIP2), *Kcna5* (K_V1.5), *Col1a* (collagen type I), *Col3a* (collagen type III), and hypoxanthine phosphoribosyltransferase (*Hprt1*;reference gene) were used. Primer sequences are listed in Supplemental Table S7 below.

Total RNA was isolated from right or left atrial appendages using a PureZOL™ RNA Isolation Reagent and the Aurum™ Total RNA Fatty and Fibrous Tissue Kit (Bio-Rad Laboratories) as per kit instructions. RNA samples were eluted from the spin column in 40 µL elution buffer. RNA yield and purity were assessed using a Nanodrop. All samples had a A_{260}/A_{280} of over 2.0 and therefore were free of DNA contamination. Next, cDNA (5 ng/µL) was synthesized using the iScript™ cDNA Synthesis Kit (Bio-Rad Laboratories). Reactions were performed in a Bio-Rad MyCycler thermal cycler using the following protocol: 5 min of priming at

25 °C followed by reverse transcription for 30 min at 42 °C then 5 min at 85 °C to inactivate reverse transcriptase.

All qPCR reactions were run in duplicate in 10 µL reactions that contained the following: 4 µL sample cDNA, 5.6 µL GoTaq® qPCR Master Mix (Promega), and 0.4 µL primers. Primers were reconstituted to a final concentration of 100 µM with nuclease free water and stored at −20 °C until use. Primers were diluted to 10 µM for qPCR reactions. RT-qPCR reactions were performed using the CFX386 Touch™ Real-Time PCR Detection System (Bio-Rad) using the following protocol: Taq polymerase was activated for 2 min at 95 °C followed by 39 cycles of denaturing for 15 s at 95 °C, annealing for 30 s at 60 °C, and extension for 30 s at 72 °C. This was followed by melt curve analysis from 65-95 °C in 0.5 °C increments. Data were analyzed using the $2^{-\Delta\Delta C_T}$ method using the CFX Manager Software version 3.1 (Bio-Rad).

Western blotting

Protein samples were extracted from the left atrial appendage. Tissue was cooled in liquid nitrogen, ground into a powder, and then incubated for 1 hour with ice-cold modified RIPA buffer that contained (in mM): 50 mM Tris, 150 mM NaCl, 25 mM sucrose, 1 mM EDTA, 1% Triton, 0,1% SDS. Protease inhibitor cocktail (Sigma-Aldrich) and 0.5 mM DTT (1,4-Dithiothreitol, Roche) were added to prevent protein degradation. Next, preparations were centrifuged for 10 min at 10,000 rpm at 4 °C and protein concentrations were measured using the Bio-Rad DC™ Protein Assay Kit II (Bio-Rad Laboratories). For K_v4.2, K_v4.3, and K_v1.5 Western blot experiments, protein samples (20 µg/lane) were separated by 7.5% SDS-polyacrylamide gels (SDS-PAGE) and transferred onto a BioTrace™ NT Nitrocellulose Transfer Membrane (VWR). For KChIP2 Western blot experiments, a protein concentration of 40 µg/lane was used and proteins were separated on a 10% SDS-PAGE gel. The membrane was blocked for 1 hour at room temperature with 1% casein in Tris-buffered saline (TBS; Bio-Rad Laboratories). Blots were incubated overnight at 4 °C with rabbit-raised primary antibodies to

K_v4.2 (1:500, Alomone Labs), K_v4.3 (1:1,000, Alomone Labs), K_v1.5 (1:500, Alomone Labs) or KChIP2 (1:500, Alomone Labs). The Western blot membranes were then washed 3 times for 10 min in 1% TBST (TBS with 1% Tween 20 (Bio-Rad Laboratories)) before secondary antibody binding. Membranes were incubated with goat anti-rabbit IgG StarBright Blue 700 (1:2,500, Bio-Rad Laboratories) fluorescent secondary antibodies for 1 hour at room temperature. In K_v4.3, KChIP2, and K_v1.5 experiments, membranes were simultaneously incubated with hFAB Rhodamine Anti-GAPDH IgG (1:5,000, Bio-Rad Laboratories) as a primary anti-GAPDH antibody was not used. Following incubation, the membrane was washed 3 times for 10 min with 1% TBST before imaging. All Western blot membranes were imaged using the ChemiDoc™ MP Imaging System (Bio-Rad Laboratories). Protein expression was normalized to GAPDH.

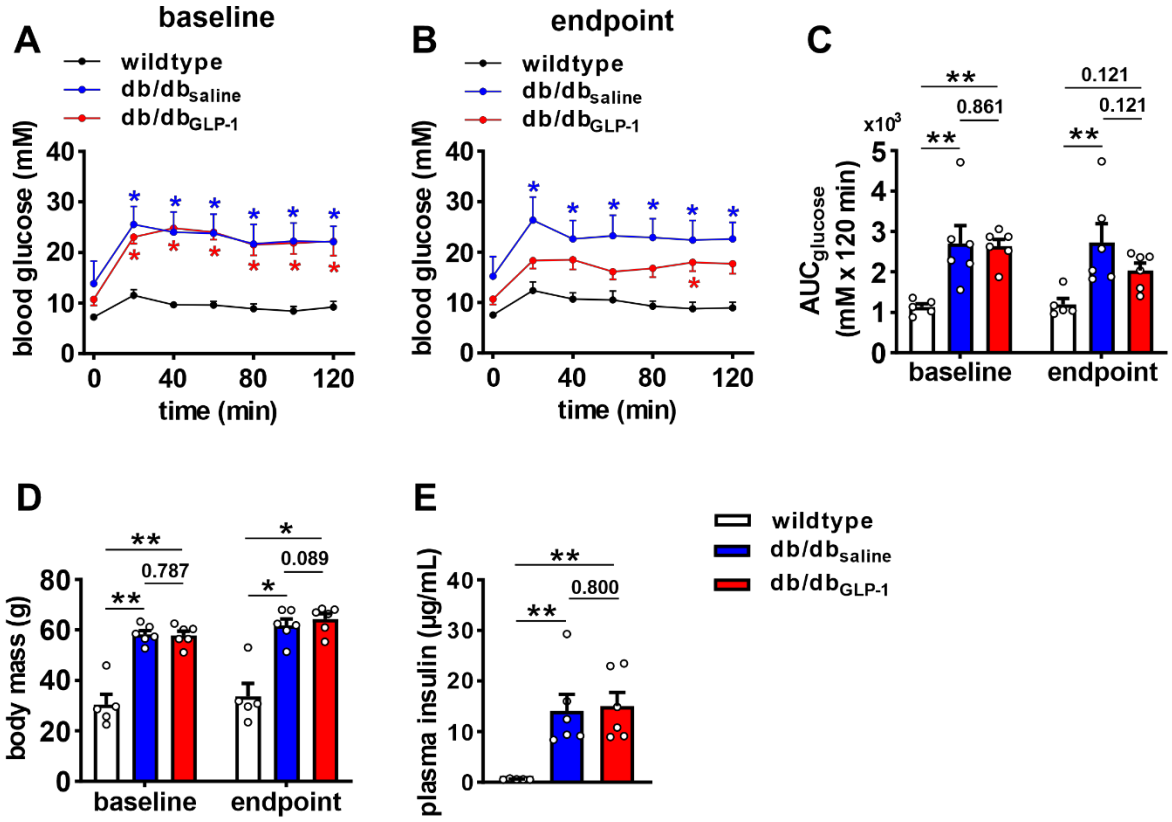

Supplemental Figure 1: Blood glucose, body mass, and plasma insulin in db/db mice treated with GLP-1 for 4 weeks. (**A and B**) Oral glucose tolerance test in wild-type, db/db$_{saline}$, and db/db$_{GLP-1}$ mice at baseline (**A**) and after 4 weeks of GLP-1 (or saline) infusion (**B**). *P < 0.05 vs wild type by two-way repeated measures ANOVA with Holm-Sidak post hoc test. (**C**) Area under the curve (AUC$_{glucose}$) for the data in panels A and B. Data analyzed by two-way repeated measures ANOVA with Holm-Sidak post hoc test. (**D**) Body mass in wild-type, db/db$_{saline}$, and db/db$_{GLP-1}$ mice at baseline and after 4 weeks of GLP-1 (or saline) treatment. Data analyzed by two-way repeated measures ANOVA with Holm-Sidak post hoc test. For panels A-D n = 5 wild-type, 6 db/db$_{saline}$, and 6 db/db$_{GLP-1}$ mice. (**E**) Plasma insulin levels in wild-type, db/db$_{saline}$, and db/db$_{GLP-1}$ mice after 4 weeks of GLP-1 (or saline) treatment. Data analyzed by one-way ANOVA with Holm-Sidak post hoc test; n = 5 mice per group.

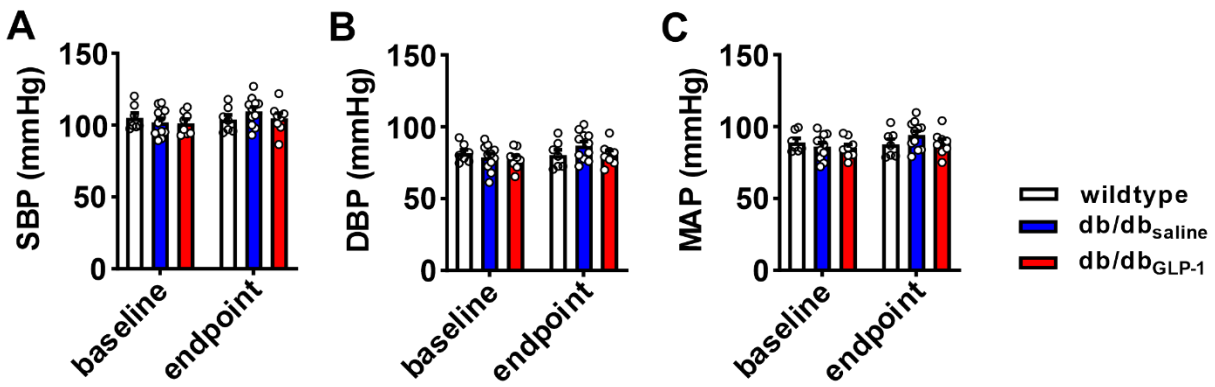

Supplemental Figure 2: Blood pressure in db/db mice treated chronically with GLP-1. (**A-C**) systolic (SBP; **A**), diastolic (DBP, **B**) and mean arterial (MAP, **C**) pressures in wild-type, db/db_{saline}, and db/db_{GLP-1} mice at baseline and after 4 weeks of GLP1 (or saline) infusion. There were no differences in blood pressure between groups or at different time points. Data analyzed by two-way repeated measures ANOVA with Holm-Sidak post hoc test; n = 7 wild-type, 11 db/db_{saline}, and 8 db/db_{GLP-1} mice.

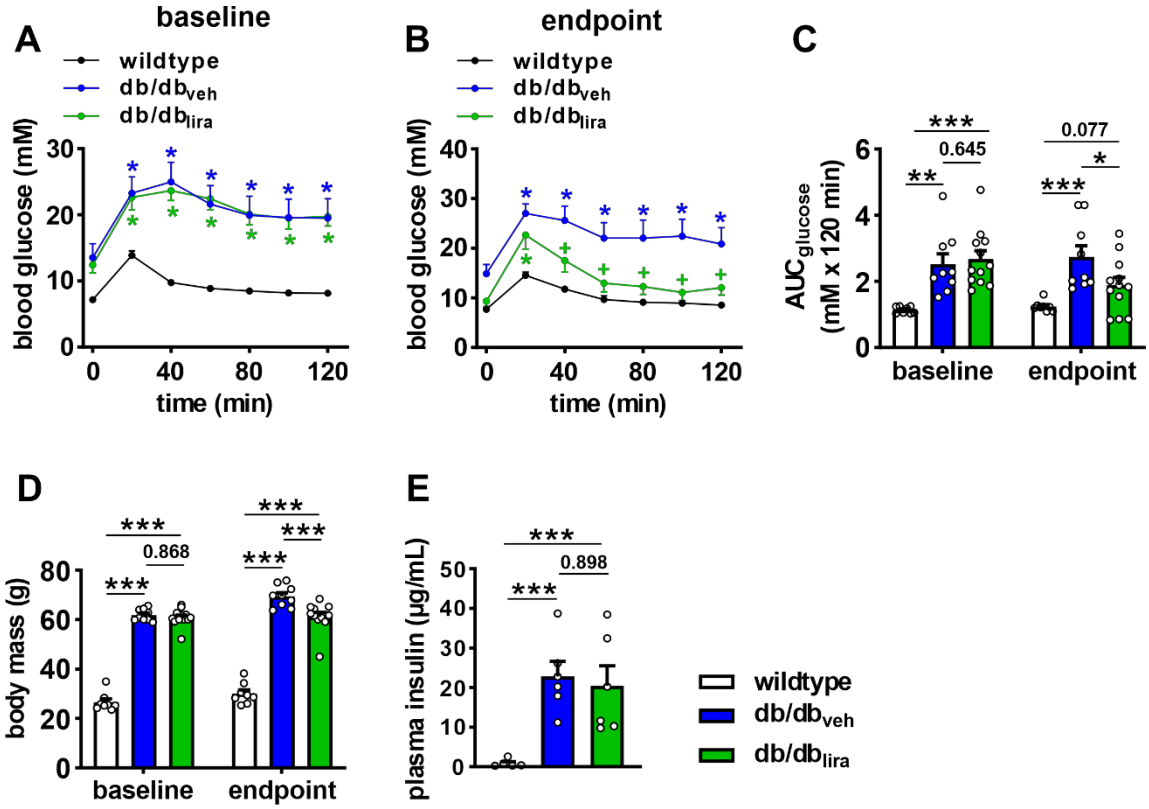

Supplemental Figure 3: Blood glucose, body mass, and plasma insulin in db/db mice treated with liraglutide for 4 weeks. (**A and B**) Oral glucose tolerance test in wild-type, db/db$_{veh}$, and db/db$_{lira}$ mice at baseline (**A**) and after 4 weeks of daily liraglutide (or vehicle) injections (**B**). $^{*}P < 0.05$ vs wild type, $^{+}P < 0.05$ vs db/db$_{veh}$ by two-way repeated measures ANOVA with Holm-Sidak post hoc test. (**C**) Area under the curve (AUC$_{glucose}$) for the data in panels A and B. Data analyzed by two-way repeated measures ANOVA with Holm-Sidak post hoc test. (**D**) Body mass in wild-type, db/db$_{veh}$, and db/db$_{lira}$ mice at baseline and after 4 weeks of liraglutide (or vehicle) injections. Data analyzed by two-way repeated measures ANOVA with Holm-Sidak post hoc test. For panels A-D n = 8 wild-type, 9 db/db$_{veh}$, and 12 db/db$_{lira}$ mice. (**E**) Plasma insulin levels in wild-type, db/db$_{veh}$, and db/db$_{lira}$ mice after 4 weeks of liraglutide (or vehicle) injections. Data analyzed by one-way ANOVA with Holm-Sidak post hoc test; n = 6 mice per group.

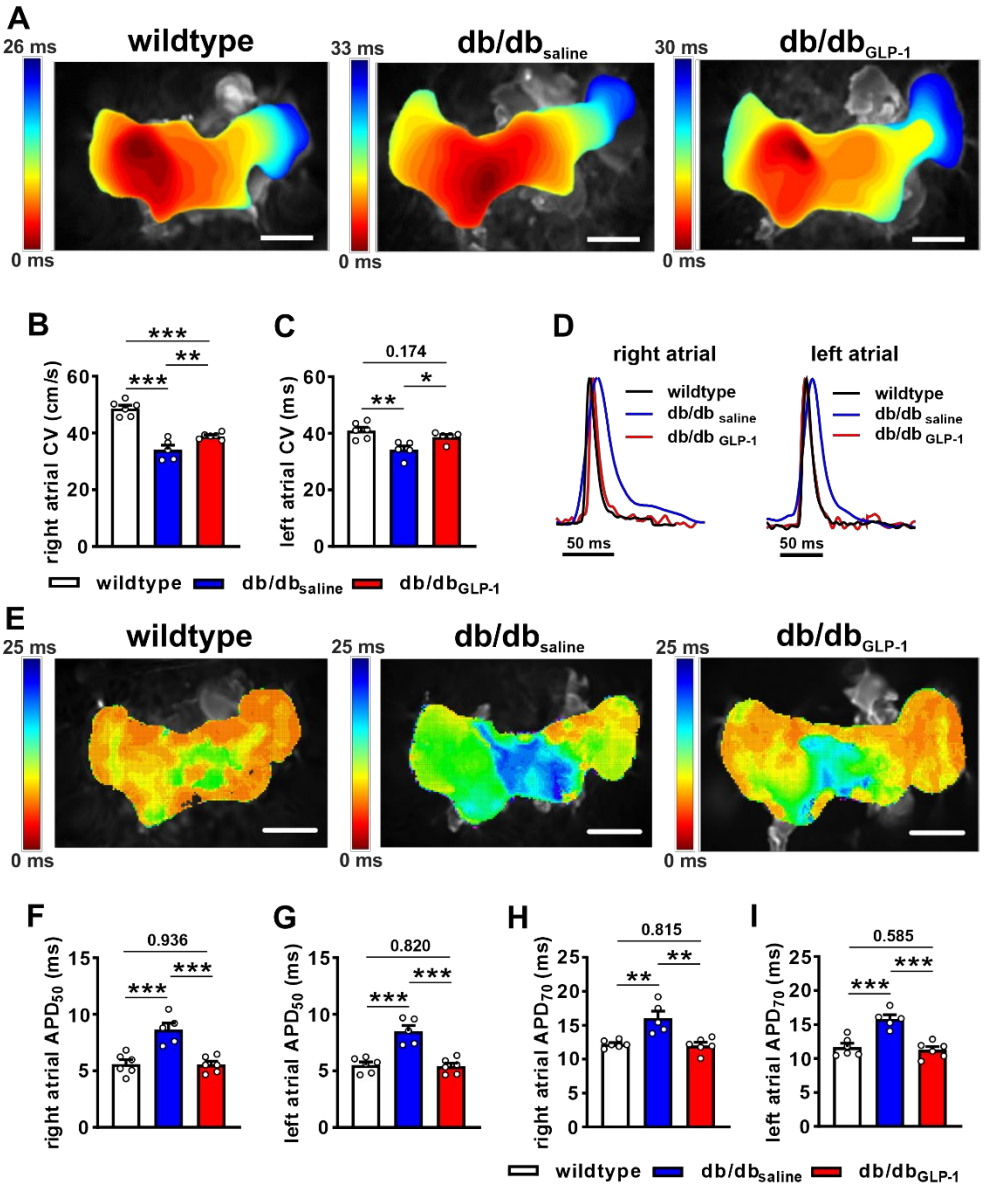

Supplemental Figure 4: Effects of chronic GLP-1 on atrial conduction and atrial optical action potential morphology in db/db hearts in sinus rhythm. (**A**) Representative activation maps in isolated atrial preparations from wild-type, db/db$_{saline}$, and db/db$_{GLP-1}$ mice in sinus rhythm. Right atrial appendage is on the left side of the image. Color scale indicates total conduction time across the preparation. Scale bar = 2 mm. (**B and C**) Summary of right atrial (**B**) and left atrial (**C**) conduction velocity (CV) in wild-type, db/db$_{saline}$, and db/db$_{GLP-1}$ mice. (**D**) Representative right atrial and left atrial optical action potentials in isolated atrial preparations from wild-type, db/db$_{saline}$, and db/db$_{GLP-1}$ mice. (**E**) Representative action potential duration maps at 50% repolarization time (APD_{50}) in atrial preparations from wild-type, db/db$_{saline}$, and db/db$_{GLP-1}$ mice. Scale bar = 2 mm. (**F and G**) Summary of right (**F**) and left (**G**) atrial APD_{50} in atrial preparations from wild-type, db/db$_{saline}$, and db/db$_{GLP-1}$ mice. (**H and I**) Summary of right (**H**) and left (**I**) atrial APD_{70} in atrial preparations from wild-type, db/db$_{saline}$, and db/db$_{GLP-1}$ mice. All summary data analyzed by one-way ANOVA with Holm-Sidak post hoc test; n = 5-6 atrial preparations per group.

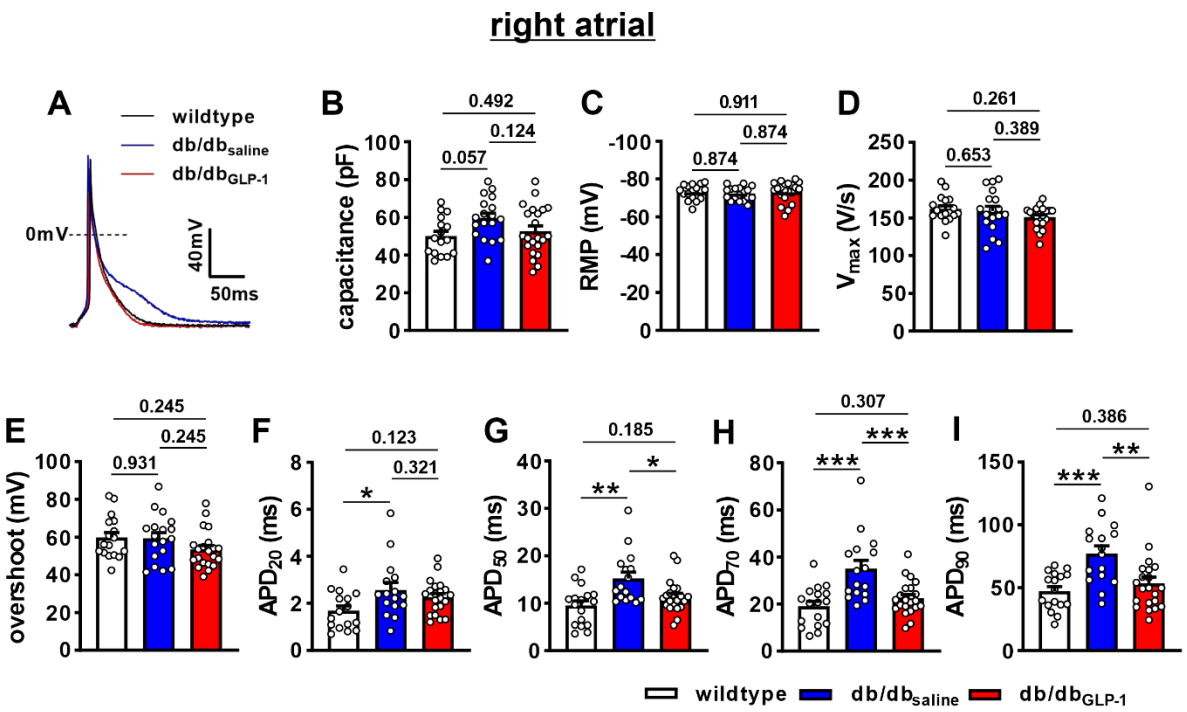

Supplemental Figure 5: Effects of chronic GLP-1 on action potential morphology in isolated right atrial myocytes in db/db mice. (**A**) Representative stimulated action potentials in right atrial myocytes isolated from wild-type, db/db$_{saline}$, and db/db$_{GLP-1}$ mice. (**B-I**) Summary data for cell capacitance (**B**), resting membrane potential (RMP, **C**), AP upstroke velocity (V_{max}, **D**), overshoot (**E**), APD_{20} (**F**), APD_{50} (**G**), APD_{70} (**H**), and APD_{90} (**I**) in isolated right atrial myocytes from wild-type, db/db$_{saline}$, and db/db$_{GLP-1}$ mice. Data analyzed by one-way ANOVA with Holm-Sidak post hoc test; n = 17 myocytes from 5 mice for wild type, 18 myocytes from 7 mice for db/db$_{saline}$, and 21 cells from 8 mice for db/db$_{GLP-1}$.

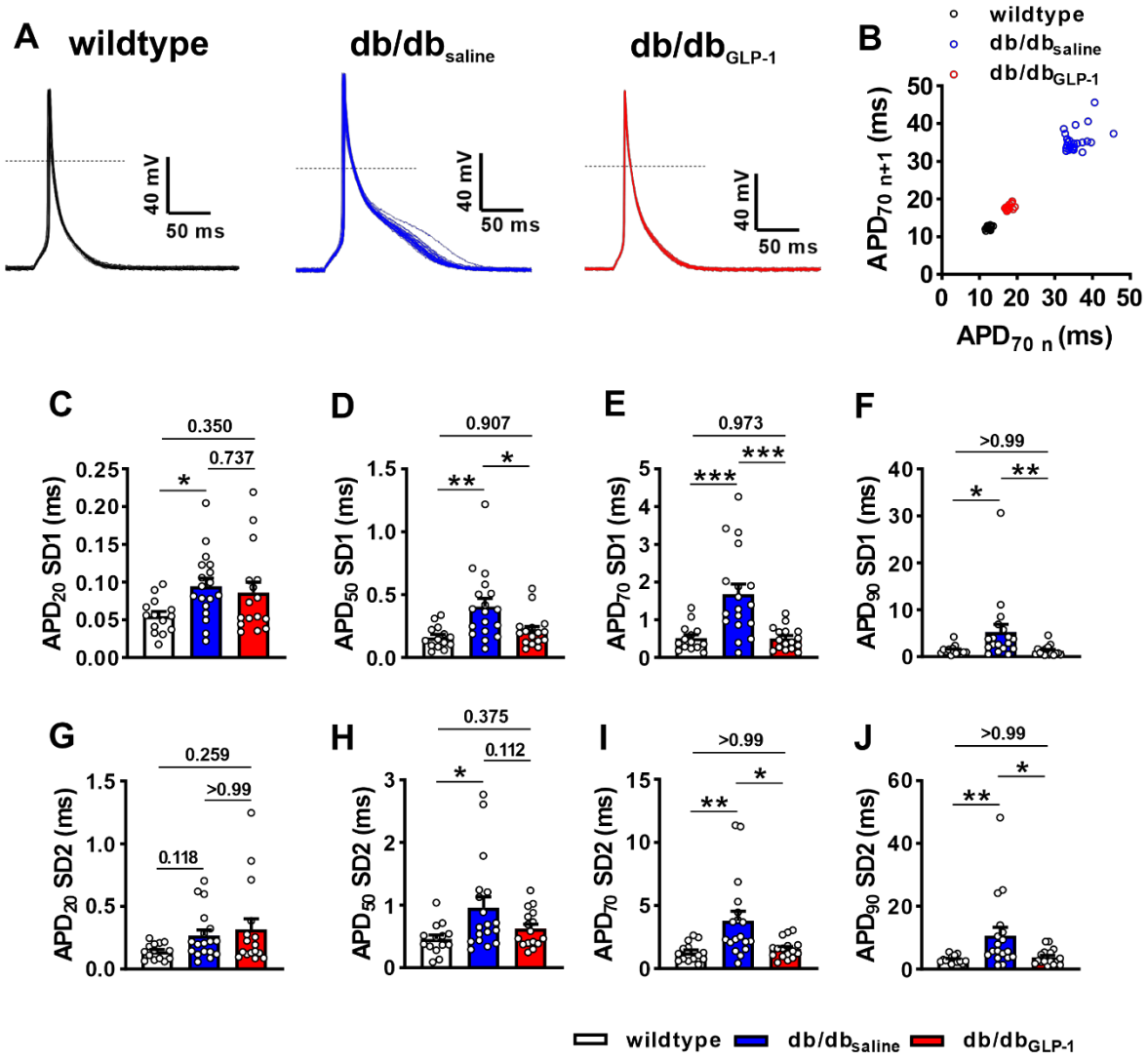

Supplemental Figure 6: Effects of chronic GLP-1 on action potential heterogeneity in right atrial myocytes in db/db mice. (**A**) Representative overlays of stimulated action potentials in isolated right atrial myocytes from wild-type, db/db$_{saline}$, and db/db$_{GLP-1}$ mice. (**B**) Representative Poincaré plot for APD$_{70}$ for stimulated APs in right atrial myocytes from wild-type, db/db$_{saline}$, and db/db$_{GLP-1}$ mice. (**C-F**) Summary of SD 1 (SD1) for APD$_{20}$ (**C**), APD$_{50}$ (**D**), APD$_{70}$ (**E**), and APD$_{90}$ (**F**) for isolated right atrial myocytes. (**G-J**) Summary of SD 2 (SD2) for APD$_{20}$ (**G**), APD$_{50}$ ($_{H}$), APD$_{70}$ (**I**) and APD$_{90}$ (**J**) for isolated right atrial myocytes. For panels C-J data analyzed by one-way ANOVA with Holm-Sidak post hoc test; n = 14 myocytes from 5 mice for wild type, 18 myocytes from 7 mice for db/db$_{saline}$, and 16 myocytes from 7 mice for db/db$_{GLP-1}$.

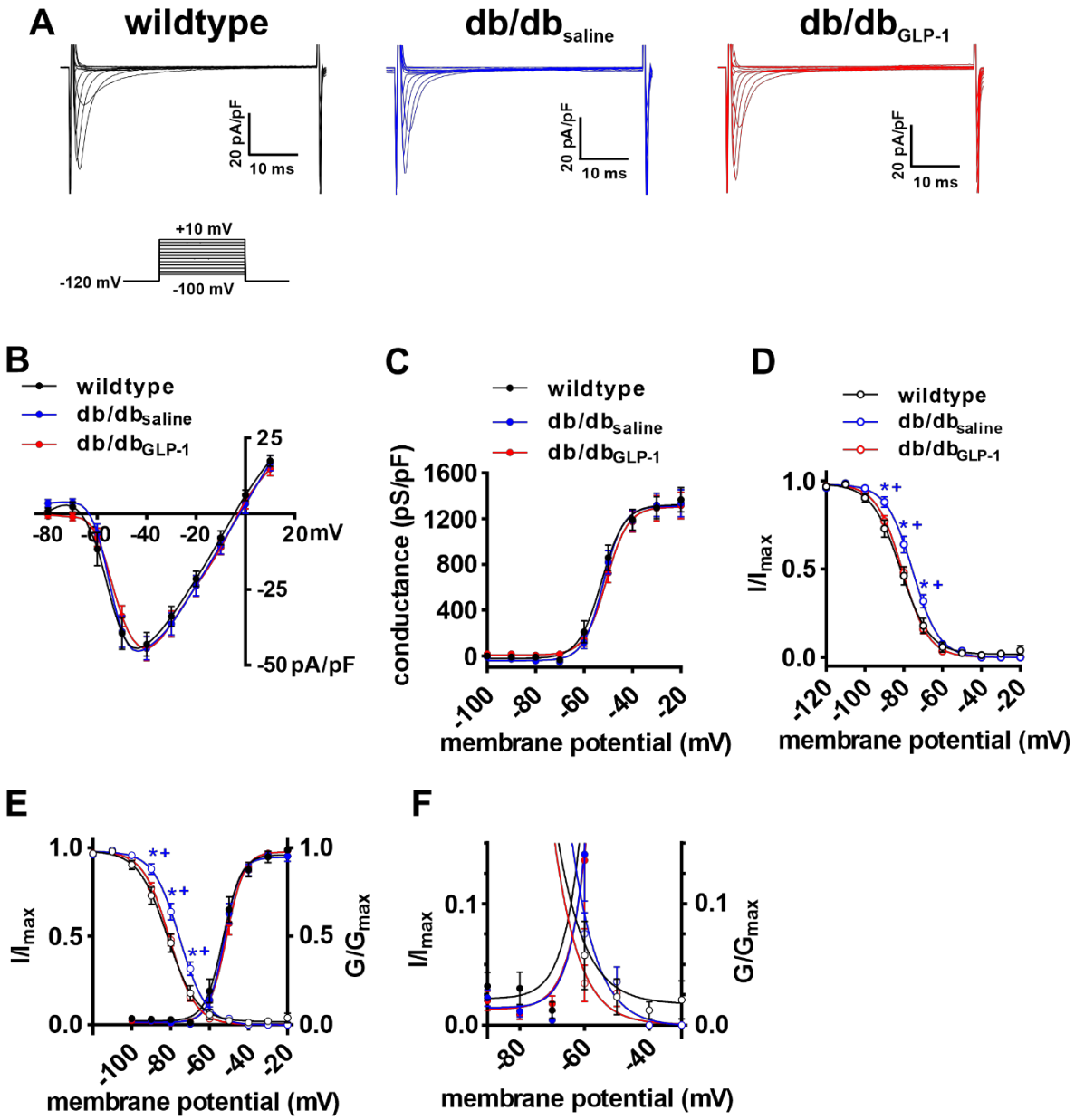

Supplemental Figure 7: Effects of chronic GLP-1 on Na^+ current in isolated right atrial myocytes from db/db mice. (**A**) Representative I_{Na} recordings in isolated right atrial myocytes from wild-type, db/db_{saline}, and db/db_{GLP-1} mice. Voltage clamp protocol shown below recordings. (**B-D**) I_{Na} IV curves (**B**), steady-state activation curves (**C**), and steady-state inactivation curves (**D**) in right atrial myocytes from wild-type, db/db_{saline}, and db/db_{GLP-1} mice. Data analyzed by two-way repeated measures ANOVA with Holm-Sidak post hoc test. There were no differences between groups in panels B and C. For panel D $^*P < 0.05$ vs wild type, $^+P < 0.05$ vs db/db_{GLP-1}. n = 10 myocytes from 3 mice for wild type, 11 myocytes from 4 mice for db/db_{saline}, and 11 myocytes from 3 mice for db/db_{GLP-1}. (**E**) Combined plots of normalized steady-state activation (G/G_{max}) and inactivation (I/I_{max}) in right atrial myocytes from wild-type, db/db_{saline}, and db/db_{GLP-1} mice. (**F**) Magnified view of steady state activation and inactivation curves illustrating window currents in wild-type, db/db_{saline}, and db/db_{GLP-1} right atrial myocytes. Refer to Supplemental Table 6 for additional analysis.

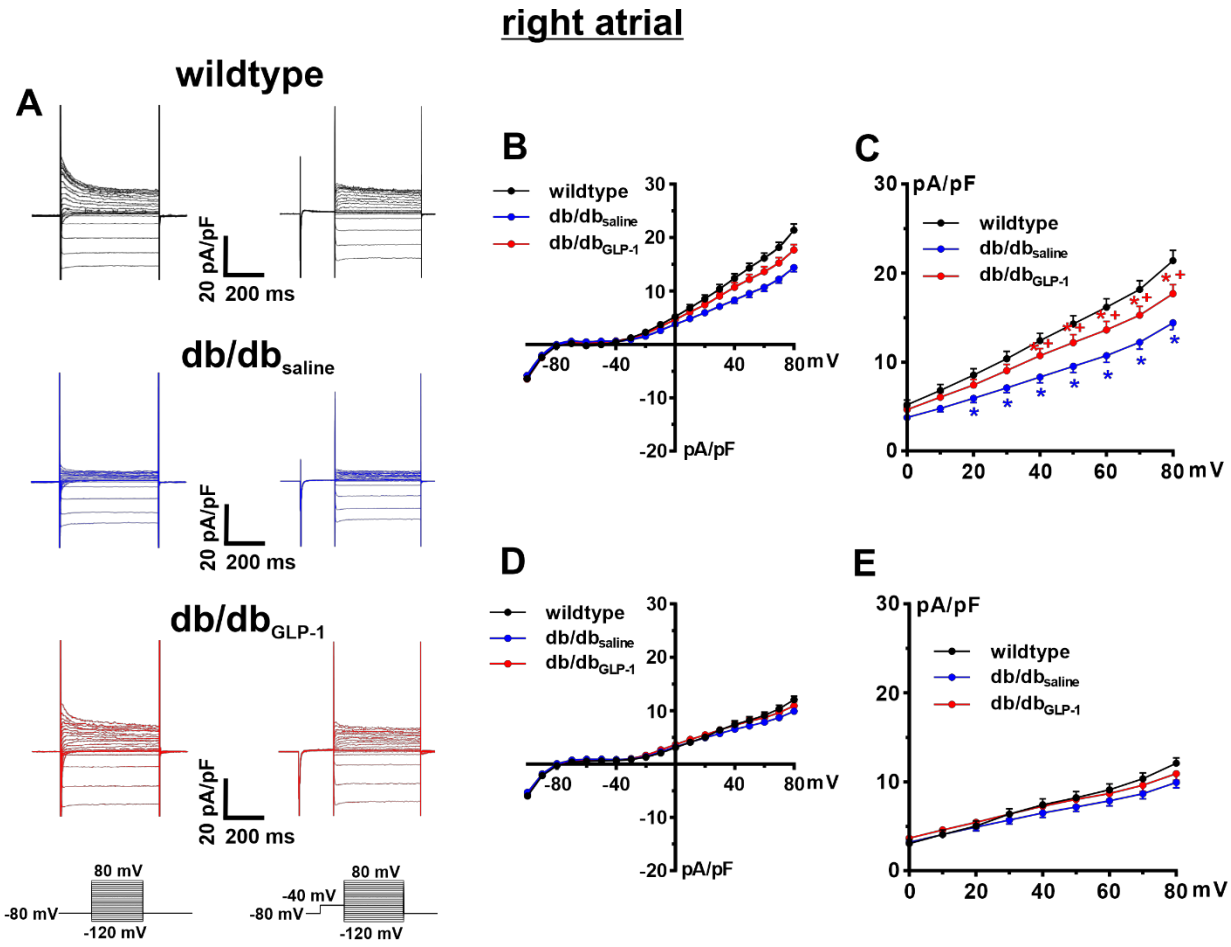

Supplemental Figure 8: Effects of chronic GLP-1 on K^+ currents in isolated right atrial myocytes in db/db mice. (**A**) Representative I_K recordings for total I_K (left) and I_K after an inactivating prepulse to −40 mV (right) in right atrial myocytes isolated from wild-type, db/db$_{saline}$, and db/db$_{GLP-1}$ mice. Voltage clamp protocols shown below recordings. (**B**) I_K IV curves measured at the peak of the total I_K recordings. (**C**) I_K IV curves (same data as panel B) showing repolarizing I_K at membrane potentials positive to 0 mV. (**D**) I_K IV curves measured at the peak of the I_K recordings after an inactivating prepulse. (**E**) I_K IV curves after an inactivating prepulse (same data as panel D) showing I_K at membrane potentials positive to 0 mV. For panel C $^*P < 0.05$ vs wild type, $^+P < 0.05$ vs db/db$_{saline}$. For panel E there were no differences between groups. Data analyzed by two-way repeated measures ANOVA with Holm-Sidak post hoc test; n = 14 myocytes from 5 mice for wild type, 16 myocytes from 8 mice for db/db$_{saline}$, and 25 myocytes from 9 mice for db/db$_{GLP-1}$. Statistical symbols shown only on panel C for clarity.

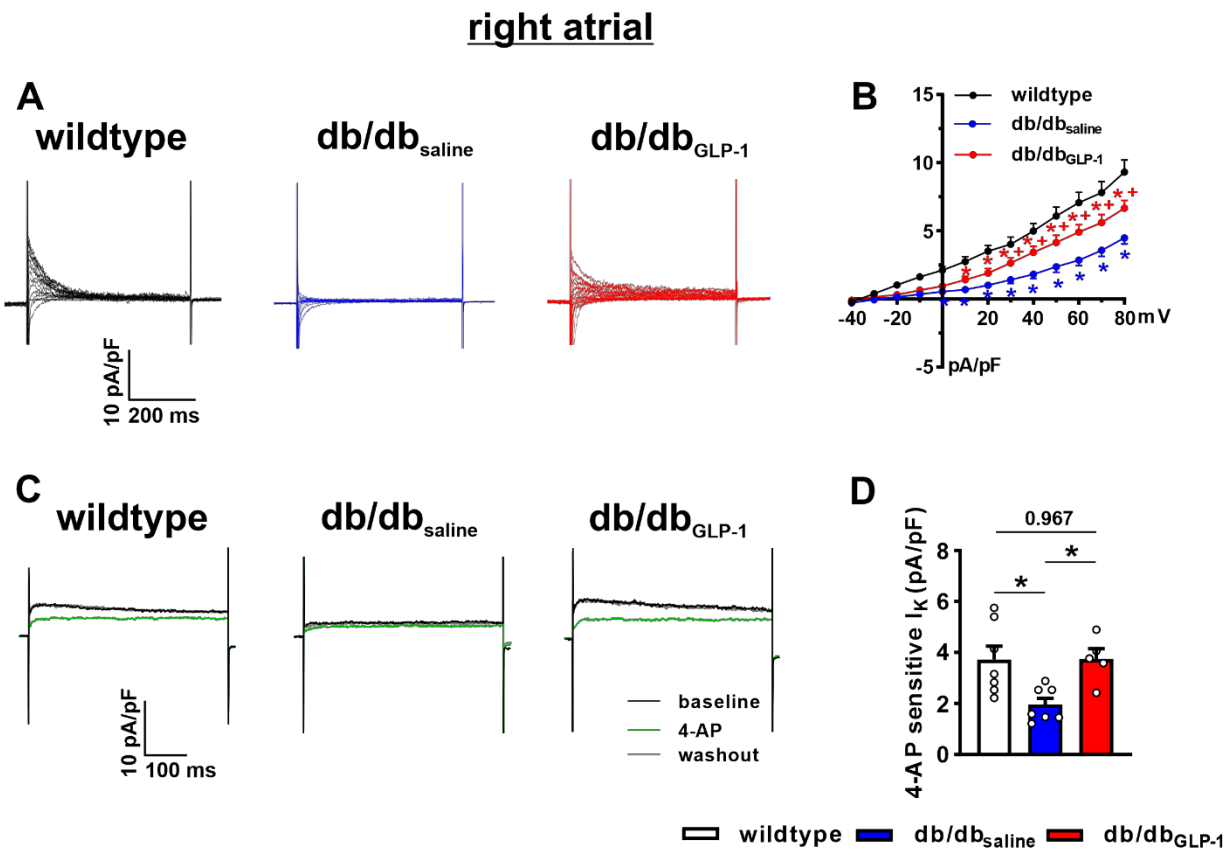

Supplemental Figure 9: Effects of chronic GLP-1 on I_{to} and 4-aminopyridine sensitive I_{Kur} in isolated right atrial myocytes in db/db mice. (**A**) Representative I_{to} recordings in isolated right atrial myocytes from wild-type, db/db_{saline}, and db/db_{GLP-1} mice generated by digitally subtracting the I_K recordings with and without a prepulse as seen in Supplemental Figure 8. (**B**) I_{to} IV curves measured as the difference current between I_K recordings with and without a prepulse as shown in Supplemental Figure 8. $^{*}P < 0.05$ vs wild type; $^{+}P < 0.05$ vs db/db_{GLP-1} by mixed-effects ANOVA with Holm-Sidak post hoc test; n =14 myocytes from 5 mice for wild type, 16 myocytes from 8 mice for db/db_{saline}, and 25 myocytes from 9 mice for db/db_{GLP-1}. (**C**) Representative I_K recordings at +30 mV showing the effects of 4-aminopyridine (4-AP; 100 μM), which inhibits $K_V1.5$-mediated I_{Kur}, in isolated right atrial myocytes from wild-type, db/db_{saline}, and db/db_{GLP-1} mice. (**D**) Summary of amplitude of 4-AP sensitive I_K in isolated right atrial myocytes from wild-type, db/db_{saline}, and db/db_{GLP-1} mice. Data analyzed by one-way ANOVA with Holm-Sidak post hoc test; n = 7 myocytes from 2 mice for wild type, 7 myocytes from 2 mice for db/db_{saline}, and 5 myocytes from 2 mice for db/db_{GLP-1}.

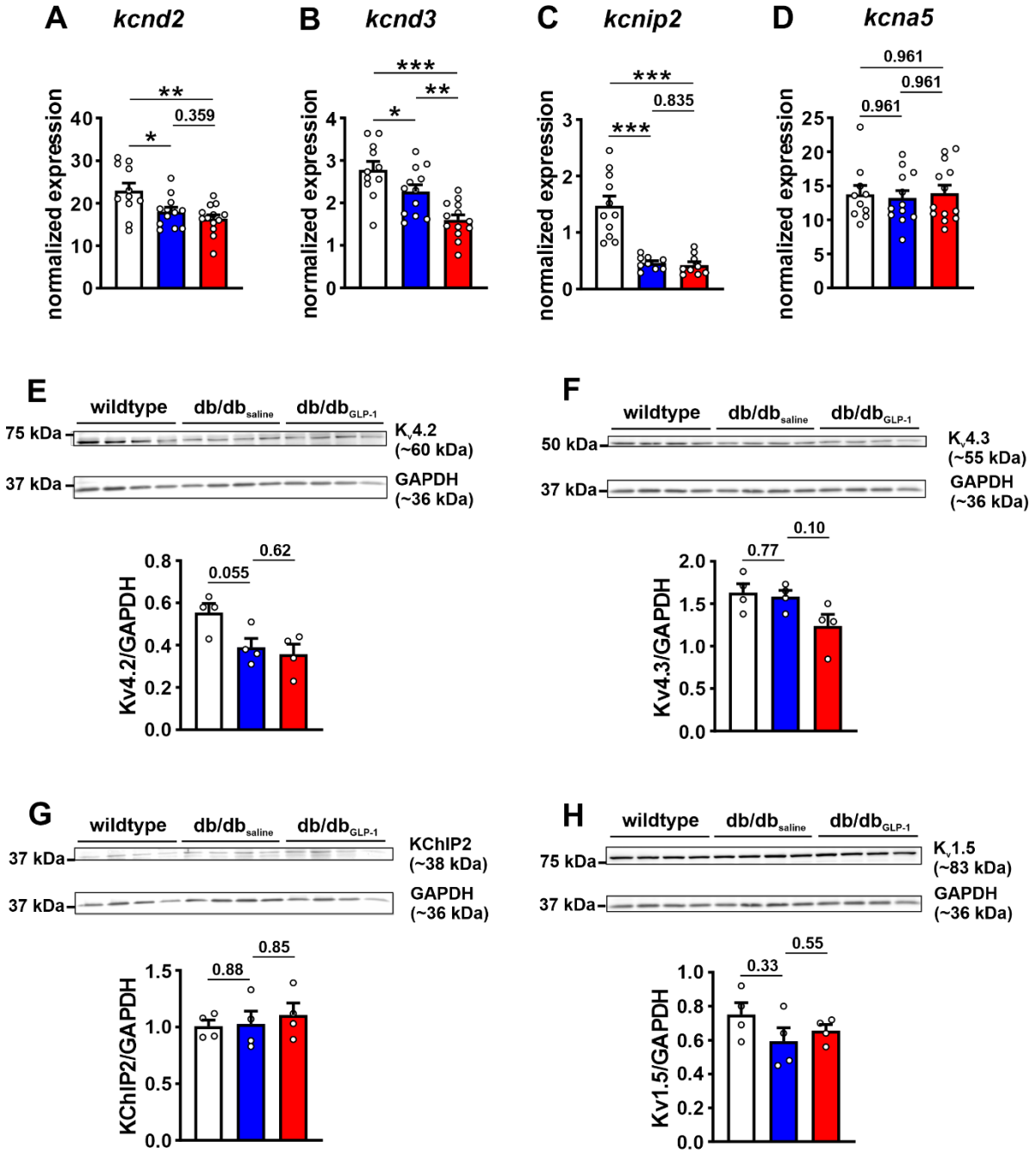

Supplemental Figure 10: Effects of chronic GLP-1 on left atrial K^+ channel mRNA and protein expression in db/db mice. (**A-D**) mRNA expression for *Kcnd2* (**A**), *Kcnd3* (**B**), *Kcnip2* (**C**), and *Kcna5* (**D**) in the left atrium in wild-type, db/db_{saline}, and db/db_{GLP-1} mice. Data analyzed by one-way ANOVA with Holm-Sidak post hoc test; n = 11 wild-type, 12 db/db_{saline}, and 13 db/db_{GLP-1} mice. (**E-F**) Representative Western blots and summary protein expression for $K_v4.2$ (**E**), $K_v4.3$ (**F**), KChIP2 (**G**), and $K_v1.5$ (**H**). Data analyzed by one-way ANOVA with Holm-Sidak post hoc test; n = 4 atria per group. Uncropped Western blots provided in Supplemental Figure 13.

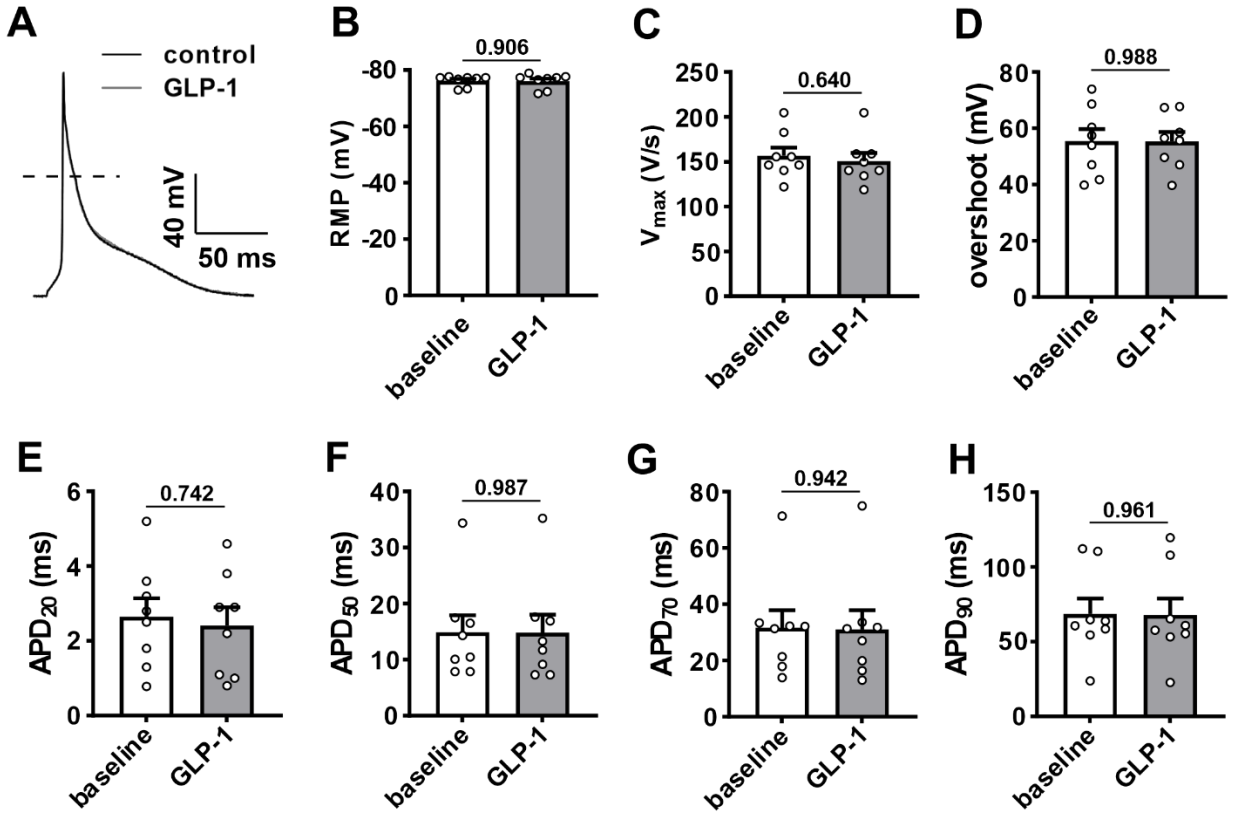

Supplemental Figure 11: Effects of acute GLP-1 on action potential morphology in isolated atrial myocytes from db/db mice. (**A**) Representative stimulated atrial action potentials in control conditions and after 5-10 min of acute superfusion with GLP-1 (100 nM). (**B-C**) Summary of the effects of acute GLP-1 on RMP (**B**), V_{max} (**C**), overshoot (**D**), APD_{20} (**E**), APD_{50} (**F**), APD_{70} (**G**), and APD_{90} (**H**) in isolated atrial myocytes from db/db mice. Data analyzed by Student's *t-test*, n = 8 myocytes from 3 mice.

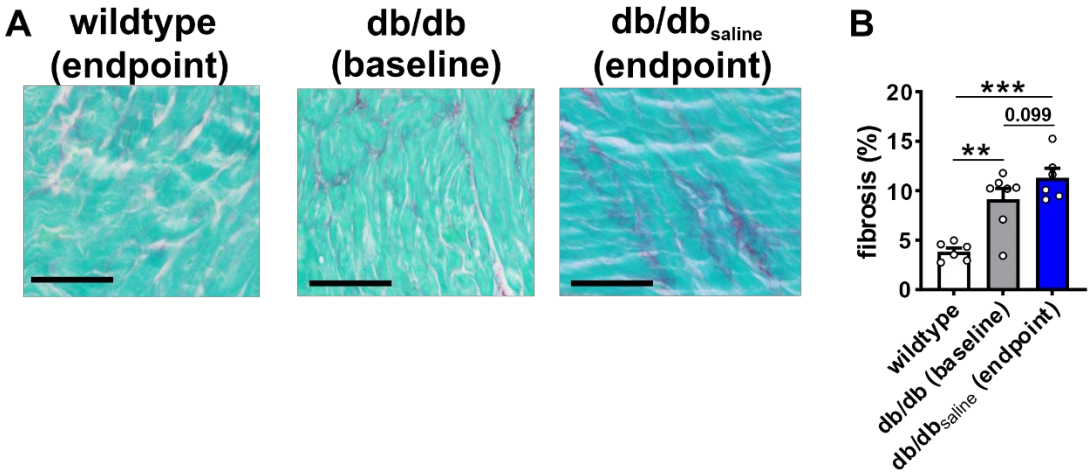

Supplemental Figure 12: Left atrial fibrosis in db/db mice. (**A**) Representative images showing patterns of interstitial fibrosis (red staining) in the left atria in wild-type mice at endpoint (ie, at time of functional studies), in db/db mice at baseline (ie, the timepoint at which GLP-1/saline infusion started), and in db/db$_{saline}$ mice at endpoint (ie, at time of functional studies). Scale bar = 50 μM. (**B**) Summary of left atrial fibrosis. Data analyzed by one-way ANOVA with Holm-Sidak post hoc test. n = 6 for wild-type endpoint, 7 for db/db$_{baseline}$, and 6 for db/db$_{saline}$ endpoint. Images and summary data for wild-type endpoint and db/db$_{saline}$ endpoint are the same as in Figure 9.

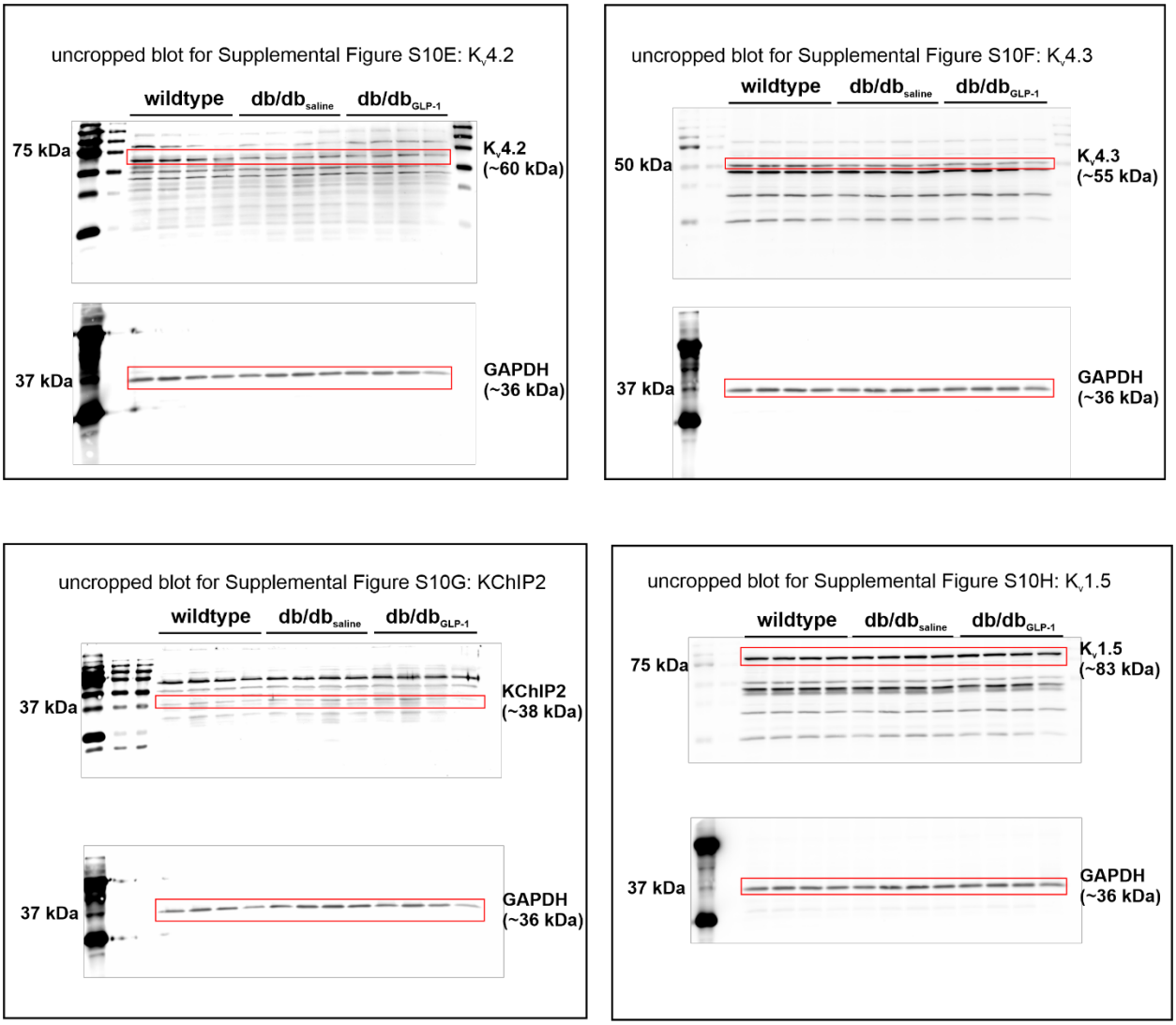

Supplemental Figure 13: Uncropped gels for Western blots.

Supplemental Table 1: Echocardiography measures in db/db mice treated with GLP-1 for 4 weeks.

	wild type	db/db_{saline}	db/db_{GLP-1}	*P* value db/db_{saline} vs wild type	*P* value db/db_{GLP-1} vs db/db_{saline}
n	11	6	8		
LVAWd (mm)	0.88 ± 0.05	0.86 ± 0.05	0.99 ± 0.04	0.98	0.21
LVPWd (mm)	0.92 ± 0.04	0.85 ± 0.05	0.97 ± 0.05	0.51	0.22
LVIDd (mm)	4.52 ± 0.07	4.47 ± 0.11	4.14 ± 0.13	0.95	0.12
LVAWs (mm)	1.32 ± 0.07	1.45 ± 0.08	1.62 ± 0.05	0.21	0.21
LVPWs (mm)	1.23 ± 0.04	1.29 ± 0.06	1.43 ± 0.06	0.46	0.16
LVIDs (mm)	3.26 ± 0.10	2.86 ± 0.09	2.53 ± 0.13	0.052	0.072
LVVd (µL)	68.2 ± 2.9	68.6 ± 2.1	68.7 ± 5.3	>0.99	>0.99
LVVs (µL)	35.5 ± 2.2	31.5 ± 1.4	32.0 ± 3.3	0.69	0.92
EF (%)	47.8 ± 2.6	54.1 ± 1.2	54.3 ± 2.0	0.21	0.96
SV (µL)	32.7 ± 2.4	37.1 ± 1.1	36.9 ± 2.4	0.48	0.97
LA $area_{max}$ (mm^2)	5.01 ± 0.33	6.79 ± 0.58	5.43 ± 0.51	0.039	0.12
LA $area_{min}$ (mm^2)	2.98 ± 0.40	3.27 ± 0.43	3.81 ± 0.33	0.64	0.64
RA $area_{max}$ (mm^2)	4.38 ± 0.31	5.42 ± 0.56	4.28 ± 0.38	0.21	0.21
RA $area_{min}$ (mm^2)	2.48 ± 0.32	3.09 ± 0.43	3.38 ± 0.57	0.59	0.67

n, number of mice, LVAW, left ventricular anterior wall thickness; LVPW, left ventricular posterior wall thickness; LVID, left ventricular internal diameter; LVV, left ventricular volume. LVAW, LVPW, LVID and LVV measurements were made during systole (s) and diastole (d). SV, stroke volume; EF, ejection fraction; LA $area_{max}$, maximum left atrial area; LA $area_{min}$, minimum left atrial area. RA $area_{max}$, maximum right atrial area; RA $area_{min}$, minimum right atrial area. Data are means ± SEM; Data analyzed by one-way ANOVA with Holm-Sidak post hoc test.

Supplemental Table 2: ECG analysis in male and female db/db mice treated with GLP-1 for 4 weeks.

	wild type	**db/db$_{saline}$**	**db/db$_{GLP-1}$**	***P*** **value db/db$_{saline}$ vs wild type**	***P*** **value db/db$_{GLP-1}$ vs db/db$_{saline}$**	***P*** **value db/db$_{GLP-1}$ vs wild type**
n	25	26	28			
HR (beats/min)	551 ± 8	508 ± 12	536 ± 9	0.007	0.071	0.26
RR interval (ms)	109.4 ± 1.60	120.0 ± 3.1	112.7 ± 1.9	0.006	0.0511	0.32
P wave (ms)	22.7 ± 0.6	30.2 ± 0.9	25.7 ± 0.7	<0.001	<0.001	0.008
PR interval (ms)	36.8 ± 0.5	41.9 ± 1.1	40.3 ± 0.8	<0.001	0.16	0.001
QRS (ms)	10.1 ± 0.4	10.9 ± 0.3	10.4 ± 0.2	0.30	0.63	0.63
QT interval (ms)	54.3 ± 2.2	57.1 ± 2.1	51.4 ± 2.5	0.61	0.22	0.61
cSNRT (ms)	27.4 ± 1.8	40.1 ± 3.5	35.0 ± 1.7	0.001	0.14	0.041
AERP (ms)	29.3 ± 0.8	35.0 ± 0.8	29.5 ± 0.9	<0.001	<0.001	0.89
AVERP (ms)	45.4 ± 1.2	47.6 ± 1.3	44.7 ± 1.6	0.48	0.36	0.70

n, sample size; HR, heart rate; cSNRT, corrected sinoatrial node recovery time; AERP, atrial effective refractory period; AVERP, AV node effective refractory period. Data analyzed by one-way ANOVA with Holm-Sidak post hoc test.

Supplemental Table 3: ECG analysis in female db/db mice treated with GLP-1 for 4 weeks.

	wild type	**db/db$_{saline}$**	**db/db$_{GLP-1}$**	***P*** **value db/db$_{saline}$ vs wild type**	***P*** **value db/db$_{GLP-1}$ vs db/db$_{saline}$**	***P*** **value db/db$_{GLP-1}$ vs wild type**
n	20	17	17			
HR (beats/min)	548 ± 9	497 ± 15	529 ± 12	0.009	0.13	0.25
RR interval (ms)	110.0 ± 1.8	122.7 ± 4.1	114.3 ± 2.6	0.009	0.10	0.30
P wave (ms)	22.5 ± 0.7	29.5 ± 1.1	25.5 ± 1.0	<0.001	0.009	0.023
PR interval (ms)	37.1 ± 0.6	40.5 ± 1.2	40.1 ± .1.2	0.065	0.79	0.065
QRS (ms)	10.0 ± 0.4	10.4 ± 0.4	10.3 ± 0.4	0.88	0.88	0.88
QT interval (ms)	55.7 ± 2.6	59.3 ± 2.7	54.0 ± 3.8	0.64	0.56	0.69
cSNRT (ms)	32.6 ± 3.6	47.0 ± 4.1	43.8 ± 4.4	0.045	0.59	0.10
AERP (ms)	29.7 ± 0.9	35.1 ± 1.2	29.1 ± 1.4	0.004	0.004	0.70
AVERP (ms)	45.5 ± 1.4	47.4 ± 1.8	46.0 ± 2.4	0.83	0.84	0.84

n, sample size; HR, heart rate; cSNRT, corrected sinoatrial node recovery time; AERP, atrial effective refractory period; AVERP, AV node effective refractory period. Data analyzed by one-way ANOVA with Holm-Sidak post hoc test.

Supplemental Table 4: ECG analysis in male db/db mice treated with GLP-1 for 4 weeks.

	wild type	**db/db$_{saline}$**	**db/db$_{GLP-1}$**	***P*** **value db/db$_{saline}$ vs wild type**	***P*** **value db/db$_{GLP-1}$ vs db/db$_{saline}$**	***P*** **value db/db$_{GLP-1}$ vs wild type**
n	5	9	11			
HR (beats/min)	563 ± 18	528 ± 19	548 ± 13	0.50	0.60	0.60
RR interval (ms)	107.0 ± 3.3	114.9 ± 4.3	110.1 ± 2.7	0.46	0.54	0.58
P wave (ms)	23.6 ± 0.9	31.4 ± 2.0	26.0 ± 0.9	0.009	0.019	0.28
PR interval (ms)	35.7 ± 0.8	43.8 ± 1.8	41.2 ± 1.1	0.015	0.191	0.078
QRS (ms)	10.2 ± 1.2	11.6 ± 0.6	10.6 ± 0.3	0.36	0.36	0.64
QT interval (ms)	48.8 ± 1.9	53.1 ± 3.2	47.4 ± 2.3	0.58	0.34	0.74
cSNRT (ms)	25.9 ± 5.9	55.4 ± 8.8	42.4 ± 5.4	0.056	0.29	0.29
AERP (ms)	27.5 ± 1.4	34.9 ± 0.5	30.2 ± 1.1	0.001	0.003	0.13
AVERP (ms)	45.3 ± 2.7	48.0 ± 2.0	42.8 ± 1.8	0.6914	0.20	0.69

n, sample size; HR, heart rate; cSNRT, corrected sinoatrial node recovery time; AERP, atrial effective refractory period; AVERP, AV node effective refractory period. Data analyzed by one-way ANOVA with Holm-Sidak post hoc test.

Supplemental Table 5: ECG analysis in db/db mice treated with liraglutide for 4 weeks.

	wild type	**db/db$_{veh}$**	**db/db$_{lira}$**	***P*** **value db/db$_{veh}$ vs wild type**	***P*** **value db/db$_{lira}$ vs db/db$_{veh}$**	***P*** **value db/db$_{lira}$ vs wild type**
n	13	16	11			
HR (beats/min)	539 ± 9	497 ± 14	523 ± 7	0.033	0.22	0.36
RR interval (ms)	111.8 ± 1.9	122.2 ± 3.7	115.0 ± 1.4	0.039	0.16	0.16
P wave (ms)	22.8 ± 1.1	29.7 ± 0.7	23.7 ± 1.2	<0.001	<0.001	0.56
PR interval (ms)	38.5 ± 0.7	46.0 ± 1.2	43.8 ± 1.1	<0.001	0.16	0.003
QRS (ms)	9.9 ± 0.5	10.7 ± 0.4	9.6 ± 0.4	0.33	0.20	0.60
QT interval (ms)	53.4 ± 2.2	56.9 ± 2.9	57.5 ± 2.0	0.88	0.88	0.88
cSNRT (ms)	25.8 ± 1.8	44.5 ± 3.3	39.5 ± 3.6	<0.001	0.25	0.009
AERP (ms)	29.6 ± 1.0	46.9 ± 3.8	39.2 ± 2.0	<0.001	0.067	0.063
AVERP (ms)	46.6 ± 1.5	53.5 ± 1.9	47.1 ± 1.4	0.015	0.025	0.83

n, sample size; HR, heart rate; cSNRT, corrected sinoatrial node recovery time; AERP, atrial effective refractory period; AVERP, AV node effective refractory period. Data analyzed by one-way ANOVA with Holm-Sidak post hoc test.

Supplemental Table 6: I_{Na} steady-state activation and inactivation parameters in db/db mcie treated with GLP-1 for 4 weeks.

	wild type	**db/db$_{saline}$**	**db/db$_{GLP-1}$**	***P*** **value db/db$_{saline}$ vs wild type**	***P*** **value db/db$_{GLP-1}$ vs db/db$_{saline}$**	***P*** **value db/db$_{GLP-1}$ vs wild type**
n (N)	10 (3)	11 (4)	11 (3)			
G_{max} (pS/pF)	1382.3 ± 106.4	1385.0 ± 106.8	1332.7 ± 112.8	0.99	0.98	0.98
$V_{1/2(act)}$ (mV)	−53.2 ± 1.6	−52.1 ± 1.4	−51.8 ± 1.5	0.89	0.91	0.89
$k_{(act)}$ (mV)	3.4 ± 0.3	4.1 ± 0.4	3.9 ± 0.2	0.38	0.65	0.46
$V_{1/2(inact)}$ (mV)	−82.0 ± 1.3	−75.8 ± 1.3	−81.5 ± 1.0	0.003	0.004	0.78
$k_{(inact)}$ (mV)	−6.1 ± 0.6	−6.0 ± 0.4	−6.1 ± 0.4	>0.99	>0.99	>0.99

n (N), number of cells (number of mice), G_{max}, maximum conductance; $V_{1/2(act)}$, voltage at which 50% of channels are activated; $k_{(act)}$, activation curve slope factor; $V_{1/2(inact)}$, voltage at which 50% of channels are inactivated; $k_{(inact)}$, inactivation curve slope factor. Data analyzed by one-way ANOVA with Holm-Sidak post hoc test, n = 10 cells from 3 mice for wild type, 11 cells from 4 mice for db/db$_{saline}$, and 11 cells from 3 mice for db/db$_{GLP-1}$.

Supplemental Table 7: PCR primers

Gene	**Gene product**	**Primer Sequence (5'→ 3')**	**Amplicon length (bp)**
Kcnd2	K_V4.2	Forward: GCAAGCGGAATGGGCTAC Reverse: TGGTTTTCTCCAGGCAGTG	126
Kcnd3	K_V4.3	Forward: CCTAGCTCCAGCGGACAAGA Reverse: CCACTTACGTTGAGGACGATCA	60
Kcnip 2	KChIP2	Forward: AACTATCCACGGTGTGCCAC Reverse: GGACATTCGTTCTTGAAGCCT	112
Kcna5	K_V1.5	Forward: TTATTCTTATGGCTGACGAGTGC Reverse: AAGGCACCAATAGTACATCCCAG	204
Col1a	Collagen type I	Forward: GCGGACTCTGTTGCTGCTTGC Reverse: GACCTGCGGGACCCCTTTGT	125
Col3a	Collagen type III	Forward: AGATCCGGGTCCTCCTGGCATTC Reverse: CTGGTCCCGGATAGCCACCCAT	194
Hprt1	Hypoxanthine phosphoribosyltransferase 1	Forward: GCAGGTCAGCAAAGAACTTATAGCC Reverse: CTCATGGACTGATTATGGACAGGAC	123